Pergamon

PII: S0191–8141(98)00020–0

Journal of Structural Geology, Vol. 20, No. 7, pp. 883 to 904, 1998

0191-8141/98 $19.00 + 0.00

Structural history of the crustal-scale Coast shear zone north of Portland Canal, southeast Alaska and British Columbia

KEITH A. KLEPEIS

Department of Geology and Geophysics, Building F05, University of Sydney, Sydney, New South Wales 2006, Australia, E-mail: keith@es.su.oz.au

MARIA LUISA CRAWFORD

Department of Geology, 101 N. Merion Avenue, Bryn Mawr College, Bryn Mawr, PA 19010, U.S.A.

and

GEORGE GEHRELS

Department of Geosciences, University of Arizona, Tucson, AZ 85721, U.S.A.

(*Received* 13 *February* 1997; *accepted in revised form* 23 *January* 1998)

Abstract—Structural, metamorphic and U–Pb geochronologic data reveal how a steep, crustal-scale shear zone influenced the evolution of the Paleogene Coast Mountains batholith during and since its emplacement. We document two distinct stages of deformation (D_3^{CSZ} and D_4^{CSZ}) that produced the Coast shear zone north of Portland Inlet. Between 65 Ma and 57 Ma, deformation now preserved within the eastern side of the Coast shear zone (D_3^{CSZ}) produced a moderately to gently, north-northeast-dipping foliation and north-east-plunging mineral lineations. D_3^{CSZ} involved dominantly east-side-up, top-to-the-southwest displacements during and after the intrusion of tabular tonalite and granodiorite plutons. Widespread crustal thickening followed by rapid exhumation, east-side-up tilting of the batholith, and decompression of rocks equilibrating at 5.6 ± 0.4 kbars, 710 ± 30°C occurred at this time. Prior to D_3^{CSZ}, deformation (D_{1-2}^{WTB}) now preserved west of the Coast shear zone resulted in tectonic imbrication of lithologically distinctive crustal fragments at 8–9 kbars, and west- to southwest-vergent ductile thrust faults before ~92 Ma. From ~57 Ma to 55 Ma, deformation in the western Coast shear zone (D_4^{CSZ}) produced a narrow, 1–2 km wide, zone comprised of a steeply-dipping to subvertical foliation that overprints and transposes all D_{1-2}^{WTB} and D_3^{CSZ} structures. D_4^{CSZ} involved bulk east-side-down displacements parallel to a steeply-plunging, down-dip sillimanite lineation and regional tilting of the batholith. This east-side-down displacement may reflect a final period of crustal readjustment and collapse following an earlier period of crustal thickening during batholith construction. The variable history of motion within the Coast shear zone appears to reflect a response to different periods of batholith development within a convergent to obliquely-convergent continental margin. © 1998 Elsevier Science Ltd. All rights reserved

INTRODUCTION

The Coast Mountains orogen of northern British Columbia and southeast Alaska records the development of a steep, crustal-scale, high-temperature (600–700°C) shear zone that evolved concomitantly with latest Cretaceous to Eocene emplacement of the Coast Mountains batholith (Crawford and Crawford, 1991; McClelland *et al*., 1992). High strain areas of the Coast shear zone (Fig. 1) coincide with the western boundary of the batholith for up to 800 km parallel to the north-northwest strike of the orogen (Hollister and Crawford, 1990; Rubin and Saleeby, 1992; McClelland *et al*., 1992). West of the Coast shear zone, exhumed middle to lower crust preserves evidence of mid-Cretaceous west- and southwest-vergent ductile thrust faulting (Crawford *et al*., 1987; Rubin *et al*., 1990; Gehrels *et al*., 1990; McClelland *et al*., 1992) with little intrusive activity between ~90 Ma and the Miocene (Cook *et al*., 1991). Multichannel seismic reflection data collected along Portland Canal show contrasts in crustal structure across the Coast shear zone suggesting that it may retain its steep orientation to the base of the crust (Hollister *et al*., 1994; Das *et al*., 1996). These relationships provide an opportunity to examine the role of a crustal-scale shear zone in controlling the evolution of a major batholith and other crustal fragments during and since their emplacement onto the North American continental margin.

The tectonic significance of the Coast shear zone during and since the emplacement of the Coast Mountains batholith has been the subject of much debate. Between Portland Inlet and the Skeena River (~54°N latitude), Crawford and Hollister (1982) interpreted the Coast shear zone as a major crustal break that separates areas of contrasting metamorphic histories. Medium to high pressure (8–9 kbars) metamorphic rocks (Crawford *et al*., 1979) on the west contrast with migmatites and assemblages indicating higher temperatures (600–700°C) but lower pressures

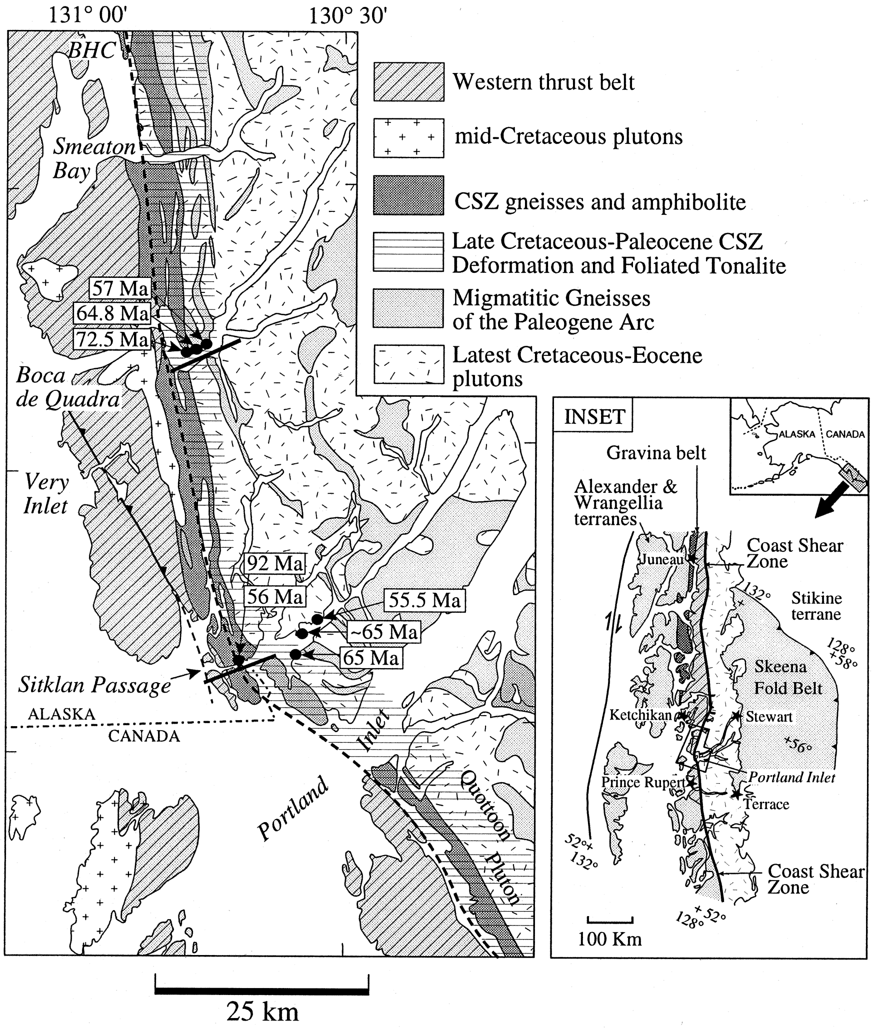

Fig. 1. Location map of the Coast shear zone near Portland Canal. Inset shows ~800 km length of the shear zone within the north Coast Mountains. Bold lines on main map are locations of transects shown in Figs 2 and 6. BHC is north Behm Canal. Black dots represent location of new U–Pb isotopic dates on zircons from intrusive rocks across the transects. Bold dashed line represents western boundary of the western Coast shear zone.

(4–5 kbars) on the east (Hollister, 1977; Selverstone and Hollister, 1980). Selverstone and Hollister (1980) and Hollister (1982) document textural relationships and K/Ar and $^{39}Ar/^{40}Ar$ cooling ages indicating rapid (2 mm/y) exhumation and decompression of the batholith and its host rocks east of the Coast shear zone. These observations suggested that the Coast shear zone played a central role in accommodating the rapid exhumation of the deep crustal portion of the Coast Mountains batholith during bulk east-side-up (reverse) displacement prior to 50 Ma (Hollister, 1982; Crawford *et al.*, 1987).

Ingram and Hutton (1994), in a study of the western edge of the Coast Mountains batholith between 54°N and 59°N latitude, concluded that contractional deformation in the Coast shear zone controlled the ascent and emplacement of numerous plutons of the Paleogene batholith and led to regional east-side-up tilting of the batholith. This interpretation was based on observations of (1) contractional deformation in the Coast shear zone involving northeast over southwest senses of displacement parallel to a steep, down-dip lineation, (2) close associations between the intrusion of numerous narrow, tabular plutons that concordantly share Coast shear zone fabrics, and (3) evidence that the fabrics within many of these plutons formed prior to complete crystallization of magmas (Ingram and Hutton, 1994).

McClelland *et al.* (1992) recognized a complex history of deformation within the Coast shear zone near Petersburg (~56.5–57°N latitude) involving both east-side-down and east-side-up, dip-slip displacements. These observations introduced the possibility of east-side-down tilting of the Paleogene batholith although the significance, locations and timing of the east-down indicators (see also Crawford *et al.*, 1989) remained unclear. McClelland *et al.* (1992) also concluded that deformation in the Coast shear zone accommodated Paleocene and Eocene exhumation of the Coast Mountains batholith but that this may have occurred during a transition from a dominantly compressional regime to one dominated by tension or transtension.

A final interpretation postulated for the Coast shear zone is that it could represent part of a major transform system that accommodated up to several thousand kilometers of northward motion along the western margin of North America between 80 Ma and 60 Ma (Umhoefer, 1987; Umhoefer *et al.*, 1989; Cowan, 1994). This interpretation is based partly on paleomagnetic data suggesting that large dextral strike-slip motion occurred parallel to the margin of western North America beween 80 Ma and 60 Ma (Beck *et al.*, 1981; Beck, 1989; Irving *et al.*, 1985, 1993). Consistent with this interpretation, the Coast shear zone has a steep orientation, is parallel to the north-northwest strike of the Coast Mountains orogen, and formed during a period (~60 Ma) when relative motion between the Kula and North American plates apparently was changing from near orthogonal convergence to dextral strike-slip or obliquely convergent motion (Engebretson *et al.*, 1985; Stock and Molnar, 1988; Lonsdale, 1988). Cowan *et al.* (1997, p. 161), however, point out that much of the proposed orogen-parallel displacement based on paleomagnetic data probably occurred prior to ~72 Ma and thus predates interpreted Paleocene ages for the Coast shear zone. Butler *et al.* (1989) also point out that tilting of the batholith may explain paleomagnetic data patterns rather than the postulated large displacements. Nevertheless, the accommodation of large orogen-parallel strike-slip displacement within the Coast Mountains during the development of the Coast shear zone is possible (Hollister and Andronicos, 1997).

Much of this controversy surrounding the significance of the Coast shear zone centers on apparently disparate interpretations of the style, kinematics and timing of deformation within the shear zone. Our focus in this paper is to establish the style, timing, sense-of-shear, and spatial distribution of different phases of deformation preserved within and adjacent to the Coast shear zone using new structural, metamorphic and U–Pb geochronologic data from sections located north of Portland Inlet. Studied localities include North Behm Canal, Smeaton Bay, Very Inlet, Boca de Quadra and Sitklan Passage (Fig. 1), all of which contain sections oriented perpendicular to the north-northwest strike of the Coast shear zone.

The significance of the studied localities, especially Sitklan Passage and Boca de Quadra, is twofold. First, these sections contain relatively small amounts of intrusive rock compared to other areas. This results in well preserved regional structural and metamorphic relationships within the shear zone with minimal local interruption by plutons and large volumes of syntectonic melt. At the same time, cross-cutting relationships involving intrusive rocks in these sections proved useful for U–Pb dating of fabrics. A second significant feature of these localities is that near Sitklan Passage and the north shore of Portland Inlet fabrics of the mid-Cretaceous western thrust belt narrow into a ~3 km wide zone at the western side of the Coast shear (Figs 1 & 2). This relationship facilitates study of cross-cutting and other structural relationships between fabrics of the Coast shear zone and those of the western thrust belt.

REGIONAL GEOLOGIC HISTORY

The Coast Mountains orogen experienced extensive crustal shortening, pluton emplacement and high grade metamorphism during Jurassic to mid-Cretaceous accretion of tectonostratigraphic terranes onto the western margin of North America (Monger *et al.*, 1982). West of the Coast shear zone, these include, from west to east, the Alexander, Taku, and Nisling terranes (Berg *et al.*, 1978; Gehrels and Berg, 1988). Exposed areas of the Alexander and Taku terranes are separated by rocks of the Late Jurassic to Cretaceous Gravina belt (Inset Fig. 1), comprising basinal turbidite sediments and mafic volcanic rocks that overlie the eastern margin of the Alexander terrane (Berg *et al.*, 1972; Gehrels and Berg, 1984; Cohen and Lundberg, 1993). Most workers (e.g. Monger *et al.*, 1982; Crawford *et al.*, 1987; Rubin and Saleeby, 1992) agree that the mid-Cretaceous tectonic assembly of the orogen occurred in a convergent setting dominated by a crustal-scale thrust belt and associated tabular syntectonic 100–90 Ma tonalitic plutons. The prior history of this terrane remains speculative. Plate motion reconstructions (e.g. Engebretson *et al.*, 1985) and geological investigations elsewhere in British Columbia and Alaska (Gehrels and Saleeby, 1987; Rusmore and Woodsworth, 1988; McClelland and Gehrels, 1990) suggest the Alexander and other terranes outboard of the North American craton were transported considerable distances along the craton margin prior to initial accretion in the Middle Jurassic.

In the Ketchikan and Prince Rupert quadrangles, rocks west of the Coast shear zone comprise the mid-Cretaceous western thrust belt, where greenschist to amphibolite facies metamorphism and deformation of the Gravina belt, and Taku and Nisling terranes produced kilometer-scale thrust sheets that verge to the southwest and west (Cook *et al.*, 1991). The Alexander terrane forms the structural basement for the thrust stack (Gehrels *et al.*, 1990; Crawford and Crawford, 1991). The highest grade metamorphic rocks of the western thrust belt lie just west of the Coast shear zone or are found in narrow aureoles adjacent to the plutons.

By the interval 65–55 Ma, high *P–T* kyanite and staurolite-bearing schists and paragneisses west of the Coast shear zone had cooled to $<250°C$ (Crawford *et al.*, 1979, 1987). Contrastingly, within and east of the Coast shear zone rocks record intense heating (600–

700°C) associated with emplacement of the Paleogene Coast Mountains batholith during convergence (Crawford and Hollister, 1982; Hollister, 1982). Many of these plutons are either steep or gently-dipping tabular bodies with margins and internal fabrics that parallel country rock foliations (e.g. Brew and Ford, 1981; Ingram and Hutton, 1994). East of the Coast shear zone latest Cretaceous to Eocene plutons intrude high grade metasedimentary and metaigneous rocks of the Central Gneiss Complex (Hutchison, 1982; Hollister and Crawford, 1990). Exhumation, decompression and cooling of the batholith and host rocks occurred prior to 50 Ma (Hollister, 1977; Selverstone and Hollister, 1980; Hollister, 1982; Crawford and Hollister, 1982).

STRUCTURAL DOMAINS AND DEFORMATION EVENTS ACROSS THE COAST SHEAR ZONE

In this paper, we describe four deformational events that affect different regions of the crust between Portland Inlet and North Behm Canal. The events are distinguished on the basis of overprinting relationships, distinctive foliation orientations, sense of shear, metamorphism, and fabric ages. The first two events (D_{1-2}^{WTB}) characterize parts of the mid-Cretaceous western thrust belt (cf. Cook *et al.*, 1991; Rubin and Saleeby, 1992; McClelland *et al.*, 1992) located at the western end of transects along Sitklan Passage, Very Inlet, Boca De Quadra and Smeaton Bay (Fig. 1). Differences in fold and fabric geometries and mineral assemblages suggests a subdivision of the western thrust belt into three domains (Fig. 2). Domains Ia and Ib occur only in the region surrounding Sitklan Passage (Fig. 2). Outside the study area, structures similar to those in domains Ia and Ib are found in the west metamorphic belt of southeast Alaska (Crawford and Crawford, 1991). Domain II represents parts of the western thrust belt traceable in a continuous belt from the south shore of Sitklan Passage to Smeaton Bay (Fig. 3).

Between Portland Inlet and North Behm Canal structural, metamorphic and geochronologic evidence presented below suggests a regional division of the Coast shear zone into western and eastern parts. Marking the western side is a narrow, 1–2 km wide, zone comprised of a steep to subvertical, intensely developed foliation that approximately coincides with the Coast Ranges megalineament of Brew and Ford (1978) and the Work channel lineament (Hutchison, 1982). This steep zone coincides with domain III (Fig. 2) and maintains its steep orientation in all of the studied transects (Fig. 3). This steep foliation was produced by a regional event (D_4^{CSZ}) that accommodated dominantly east-side-down shear between ~57 and 55 Ma. Contrasting with the west side, the eastern Coast shear zone contains a moderately to gently, northeast-dipping to east-dipping foliation that was produced by an event (D_3^{CSZ}) involving east-side-up, top-to-the-southwest transport between 65 Ma and 57 Ma. Structural domain IV coincides with the eastern Coast shear zone and includes parts of the Tertiary tonalite intrusive complex and migmatites.

THE WESTERN THRUST BELT (D_{1-2}^{WTB})

Mid-crustal, west- and southwest-vergent thrust faulting and folding

Adjacent to the Coast shear zone, D_{1-2}^{WTB} fabric elements are best exposed along western Sitklan Passage where the western thrust belt between the Alexander terrane and the Coast shear zone is very well exposed and narrows to ~3 km. Here, west- and southwest-vergent thrust faults are marked by narrow, 10–15 m wide, zones of chaotically deformed quartz veins and semi-brittle disruption of ductile fabrics. *S–C* fabrics, en échelon quartz veins, *C′* shear bands, and asymmetric tails (σ-type) on garnet porphyroblasts consistently indicate east over west displacement within these zones.

Inverted metamorphic gradients and changes in bulk composition across east-dipping thrusts strengthen interpretations of west- and southwest-directed transport and imbrication of lithologically distinctive crustal packages. East of Tingberg Island (Fig. 2), biotite grade meta-graywackes (domain Ib) lie below deformed garnet-bearing amphibolites and quartz-muscovite schists on Kanagunut Island (domain II, Fig. 2). These rocks are, in turn, tectonically overlain by high *P–T* kyanite + staurolite schists (domain II, Fig. 2) that formed at pressures of ~8 kbars at roughly 30 km depth (cf. Crawford *et al.*, 1979, 1987; Cook *et al.*, 1991).

Abrupt changes in fold and foliation geometries across thrust zones also support tectonic imbrication west of the Coast shear zone. Within Triassic marbles and calcareous metasediments of structural domain Ia (Fig. 2), a composite foliation (S_0/S_1^{WTB}) defined by primary compositional layering, the preferred shape orientation of elongate calcite and quartz aggregates, and the alignment of minor platy minerals is deformed by doubly-plunging, tight inclined folds (F_2^{WTB}). These folds display Type 1 interference patterns in outcrop (Figs 4a & 5a). The folds are overturned to the west and southwest in a manner consistent with west and southwest directions of tectonic transport during D_{1-2}^{WTB}. Boudinage of some quartz veins near the contact between marbles and rhyolite suggests that a northeast-plunging (~60°) extensional direction occurred sometime during deformation despite the lack of a strong mineral lineation in these rocks.

In meta-greywacke turbidites within domain Ib (Fig. 2), second generation structures (F_2^{WTB},

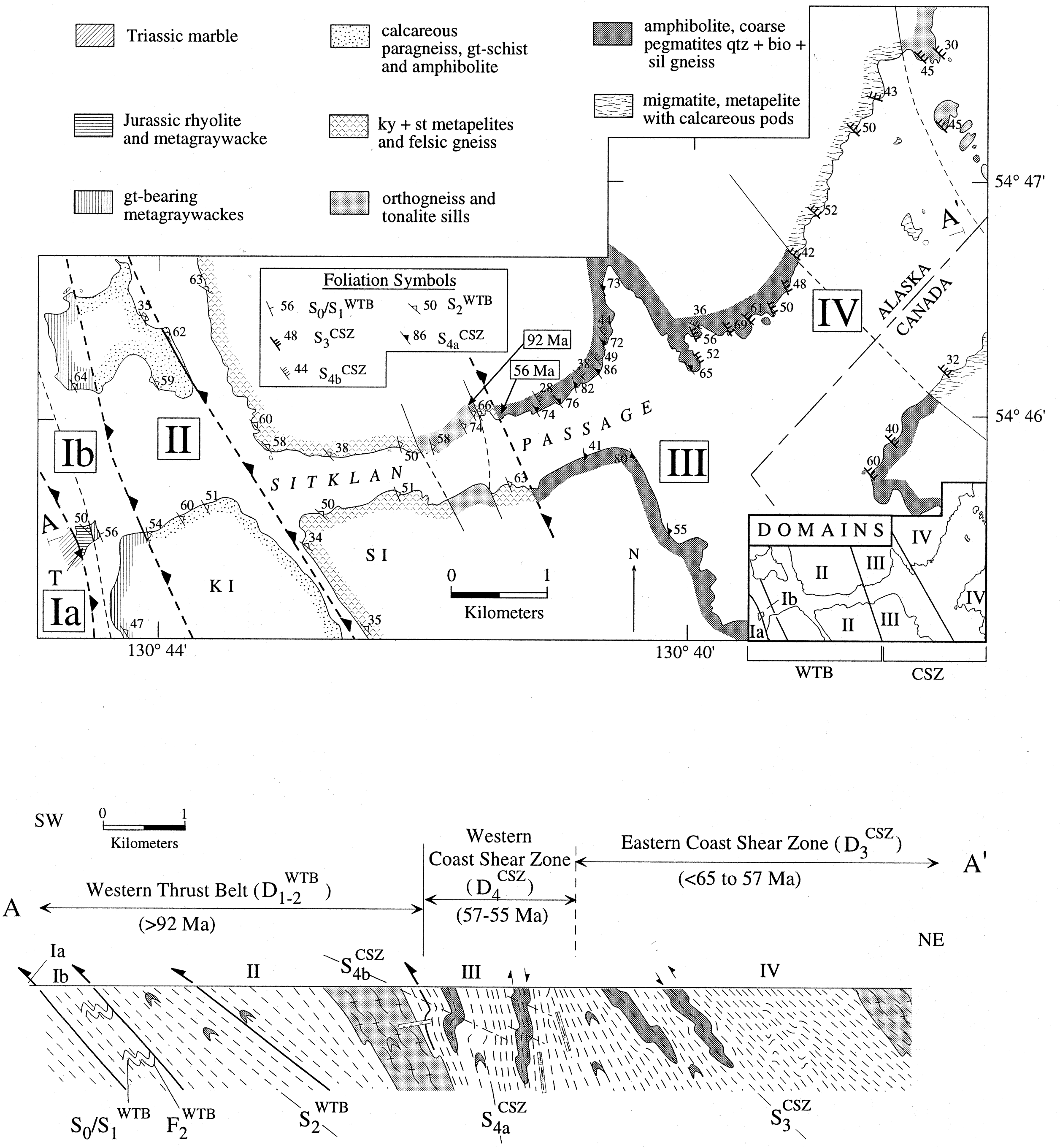

Fig. 2. Structural and lithologic map and structural cross section showing fabric elements and structural variations across the Coast shear zone along Sitklan Passage. See Fig. 1 for section location. Inset shows location of structural domains. Structural domains Ia, Ib and II correspond to the western thrust belt (D_{1-2}^{WTB} events), domain II corresponds to the western Coast shear zone (D_4^{CSZ} event), and domain IV corresponds to the eastern Coast shear zone (D_3^{CSZ} event). T is Tingberg Island, KI is Kanagunut Island, SI is Sitklan Island. Cross section location is shown as A–A′. Bold lines are thrusts, dashed where location is approximate. Boxed ages are U–Pb isotopic dates on zircons from a pegmatite (samples 94-31 and 94-32) from the western boundary of the western Coast shear determined in this study.

L_2^{WTB} and S_2^{WTB}) form the dominant fabric elements. In addition to compositional variations, the occurrence of a steeply north- to northeast-dipping cleavage (S_2^{WTB}) and gently inclined, overturned, west- and southwest-vergent folds (F_2^{WTB}) distinguish domain Ib from domain Ia (Fig. 5b). F_2^{WTB} folds deform a composite fabric (S_0/S_1^{WTB}) defined by alternating silty and sandy layers and a bedding-parallel cleavage. F_2^{WTB} axes and an intersection lineation (L_{2i}^{WTB}) defined by the intersection between S_2^{WTB} and S_0/S_1^{WTB}, plunge moderately to the east (Fig. 4), slightly obliquely to the orientation of F_2^{WTB} fold axes in the underlying

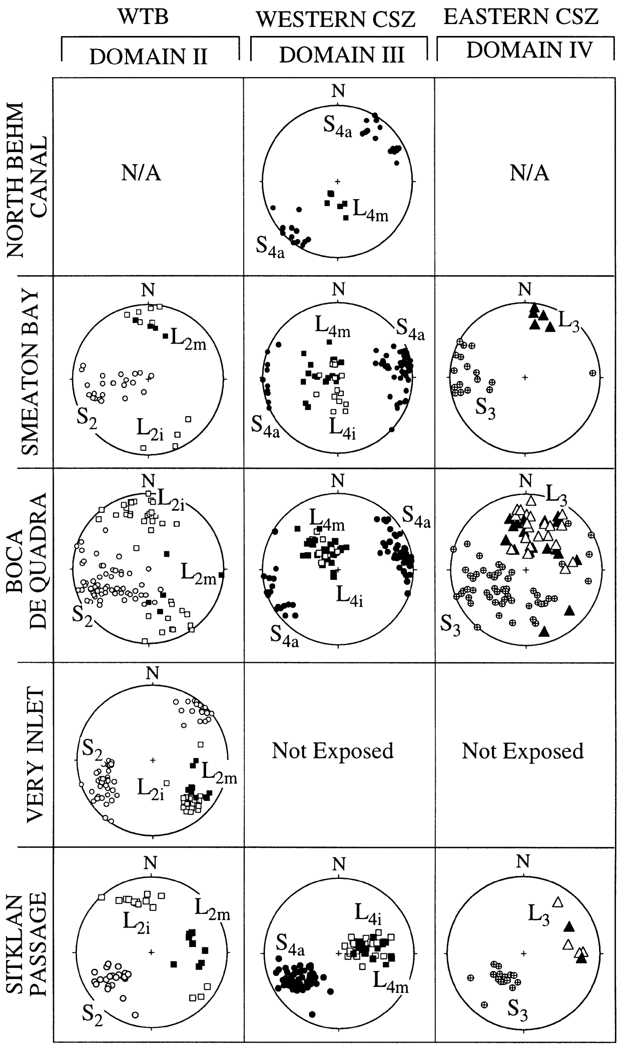

Fig. 3. Compilation of lower-hemisphere, equal-area stereoplots that show structural data from the five transects of the Coast shear zone examined in this study. North Behm Canal (top row of stereoplots) is the northernmost locality studied, Sitklan Passage (bottom row of stereoplots) is the southernmost locality. See Fig. 1 for transect locations. The left column contains data from the western thrust belt (domain II) including poles to S_2^{WTB} foliations (white circles), $L_{2\,m}^{WTB}$ mineral lineations (filled squares) and L_{2i}^{WTB} intersection lineations and F_2^{WTB} fold axes (white squares). The center column contains data from the western Coast shear zone (domain III) including poles to S_{4a}^{CSZ} (black circles), $L_{4\,m}^{CSZ}$ mineral lineations (black squares) and L_{4i}^{CSZ} intersection lineations (white squares). The right column contains data from the eastern Coast shear zone (domain IV) including poles to S_3^{CSZ} (crossed circles), $L_{3\,m}^{CSZ}$ mineral lineations (black triangles) and L_{3i}^{CSZ} intersection lineations (white triangles). See text for discussion.

marbles. S_2^{WTB} is oriented approximately axial planar to the F_2^{WTB} folds (Fig. 4b) and is refracted across sedimentary layers of different composition.

East and structurally above biotite-grade supracrustal rocks of domains Ia and Ib, the main fabric of domain II, is composed of two subparallel foliations that maintain moderately to gently-dipping orientations between Sitklan Passage and Smeaton Bay (Fig. 3). The first foliation is a gneissic foliation (S_1^{WTB}), recognizable as discontinuous compositional layering (from < 1 cm to > 0.5 m thick), that is folded into tight to isoclinal, reclined to recumbent minor folds (F_2^{WTB}). F_2^{WTB} fold axes and L_{2i}^{WTB} intersection lineations plunge gently north-northwest and southeast (Fig. 3). Many of the F_2^{WTB} folds are intrafolial, almost all are overturned, asymmetric and southwest-vergent. Along the axial planes of F_2^{WTB} folds, a second foliation (S_2^{WTB}) is defined by the preferred shape orientation of lenticular mineral aggregates and aligned biotite and hornblende. In meta-pelitic layers, S_2^{WTB} is a coarse schistosity subparallel to compositional layering that cuts through F_2^{WTB} fold hinges.

On S_2^{WTB} foliation planes, a weak, moderately east- to east-southeast-plunging mineral lineation ($L_{2\,m}^{WTB}$) is defined by streaks of white mica, quartz and plagioclase aggregates, and quartz and biotite strain shadows on garnet porphyroblasts. Down-dip extension parallel to $L_{2\,m}^{WTB}$ is evidenced by boudinaged amphibolite layers in some localities. Where both L_{2i}^{WTB} and $L_{2\,m}^{WTB}$ are present, they typically are not parallel (Fig. 3). The direction of extension indicated by $L_{2\,m}^{WTB}$ parallels the direction of extension interpreted for domains Ia and Ib along western Sitklan Passage. These geometric relationships imply that D_{1-2}^{WTB} deformation in domains Ia, Ib and II may have been progressive and/or occurred within similar kinematic displacement fields.

THE EASTERN COAST SHEAR ZONE (D_3^{CSZ})

Structure of D_3^{CSZ} *fabric elements*

East of the steep western part of the Coast shear zone, three main structural features form the distinguishing characteristics of structural domain IV. The first feature is the gently to moderately northeast-

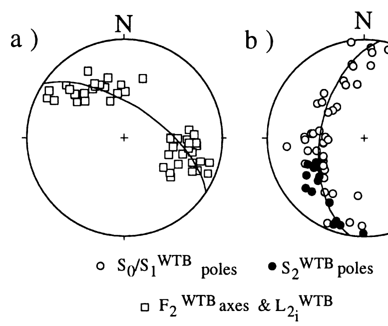

Fig. 4. Lower-hemisphere, equal-area stereoplots of structural data from structural domain Ia (a) and domain Ib (b) on Tingberg Island, western Sitklan Passage. See Fig. 2 for location of structural domains. Stereoplot (a) shows F_2^{WTB} fold axes and L_{2i}^{WTB} intersection lineations associated with doubly plunging folds, southwest-vergent folds of the western thrust belt. Great circle represents the average northeast-dipping axial plane of the F_2^{WTB} folds. Stereoplot (b) shows girdle pattern of poles to the composite S_0/S_1^{WTB} fabric. Great circle is the best fit plane to the girdle. The pole to this great circle parallels the orientation of east-plunging F_2^{WTB} fold axes (boxes). See text for discussion.

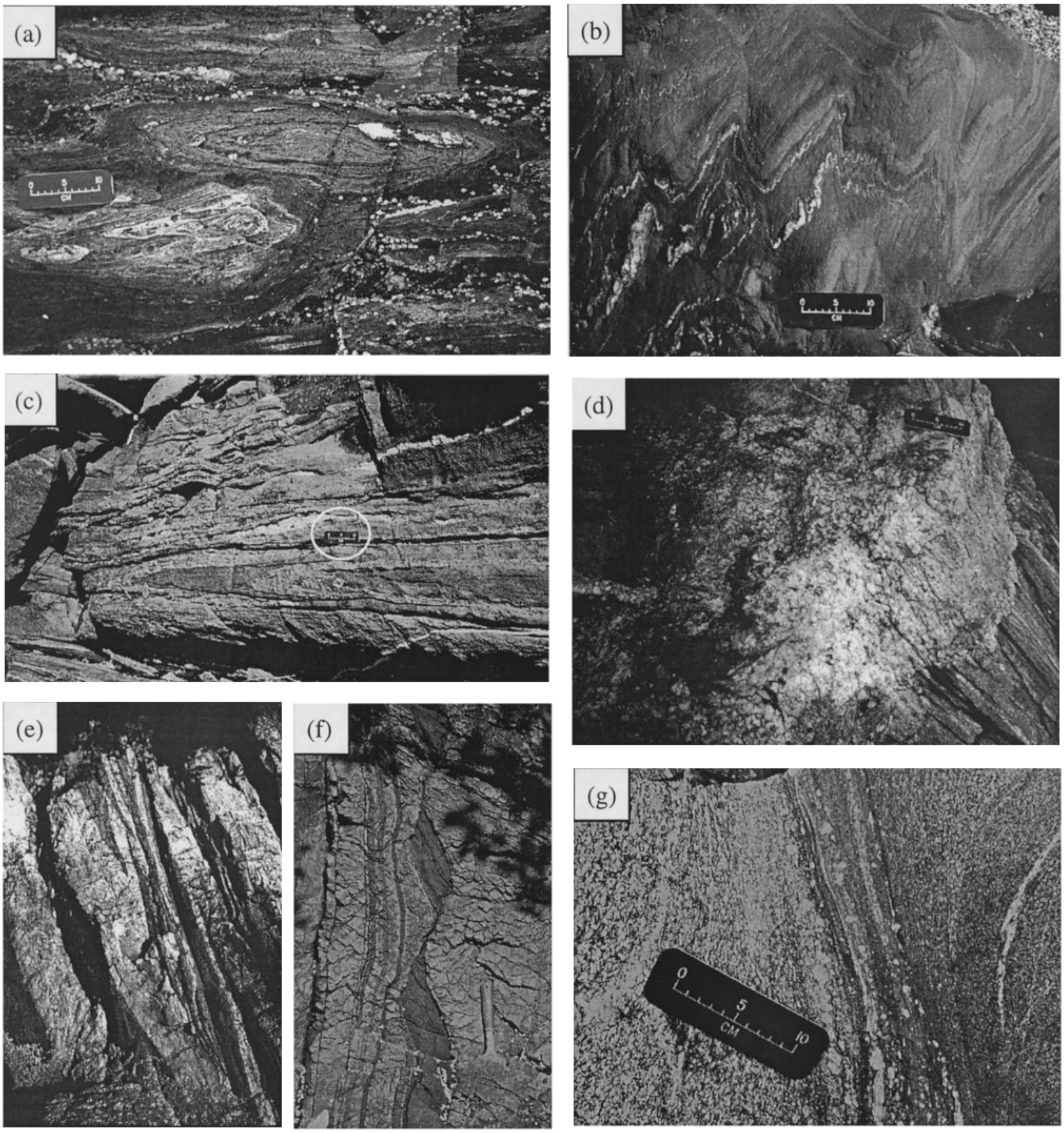

Fig. 5. (a) Type I interference fold pattern from Tingberg Island (structural domain Ia) in western Sitklan Passage. Folds (F_2^{WTB}) deform a composite S_0/S_1^{WTB} foliation in interlayered marbles and turbidites; view is to northeast. (b) Southwest-vergent (to the upper right) F_2^{WTB} folds of a composite S_0/S_1^{WTB} foliation in meta-graywackes (in domain Ib) on Tingberg Island, in western Sitklan Passage. (c) Tight to isoclinal, steeply-plunging F_{4a}^{CSZ} folds and axial planar S_{4a}^{CSZ} foliation in domain III of the western Coast shear zone. View is perpendicular to $L_{4\ m}^{CSZ}$ mineral lineations and perpendicular to the S_{4a}^{CSZ} foliation on a horizontal surface; circle shows 10 cm scale. (d) Weakly deformed pegmatite at the western edge of the western Coast shear zone (domain III) that is discordant to, but also contains, the S_{4a}^{CSZ} foliation of the western Coast shear zone. Pegmatites displaying this relationship yield ~57–55 Ma zircon dates. (e) Strongly foliated and folded (F_{4b}^{CSZ}) pegmatites within the center of the western Coast shear zone. Note alignment of pegmatites parallel to the S_{4a}^{CSZ} foliation. (f) Asymmetric boudinage of amphibolite layer within subvertical S_{4a}^{CSZ} foliation of western Coast shear zone. West is to the right. (g) Minor D_4^{CSZ} shear zone from domain IV of the eastern Coast shear zone, Boca de Quadra. See text for discussion.

to east-dipping orientation of the main foliation (S_3^{CSZ}) contained in migmatitic gneisses and schists (Figs 2 & 3). The second feature is a gently to moderately north- to east-plunging mineral lineation (L_3^{CSZ}). The third feature is the occurrence of tabular tonalite and granodiorite plutons ranging from strongly deformed to largely undeformed. Deformation that produced the L_3^{CSZ}–S_3^{CSZ} fabric of domain IV constitutes the

D_3^{CSZ} event of the eastern Coast shear zone. East of domain IV in the studied transects (Fig. 6) migmatites, large volumes of orthogneiss and complex fabric orientation changes occur. Here, foliations generally dip moderately to steeply north and northeast, and lineations are poorly developed.

L_3^{CSZ} mineral lineations in domain IV are defined by coarse prismatic sillimanite, coarse-grained hornblende, and aligned biotite and quartz–feldspar aggregates. Boudinage of amphibolite layers parallel to L_3^{CSZ} mineral lineations indicates that this lineation represents a true stretching lineation. These mineral lineations,

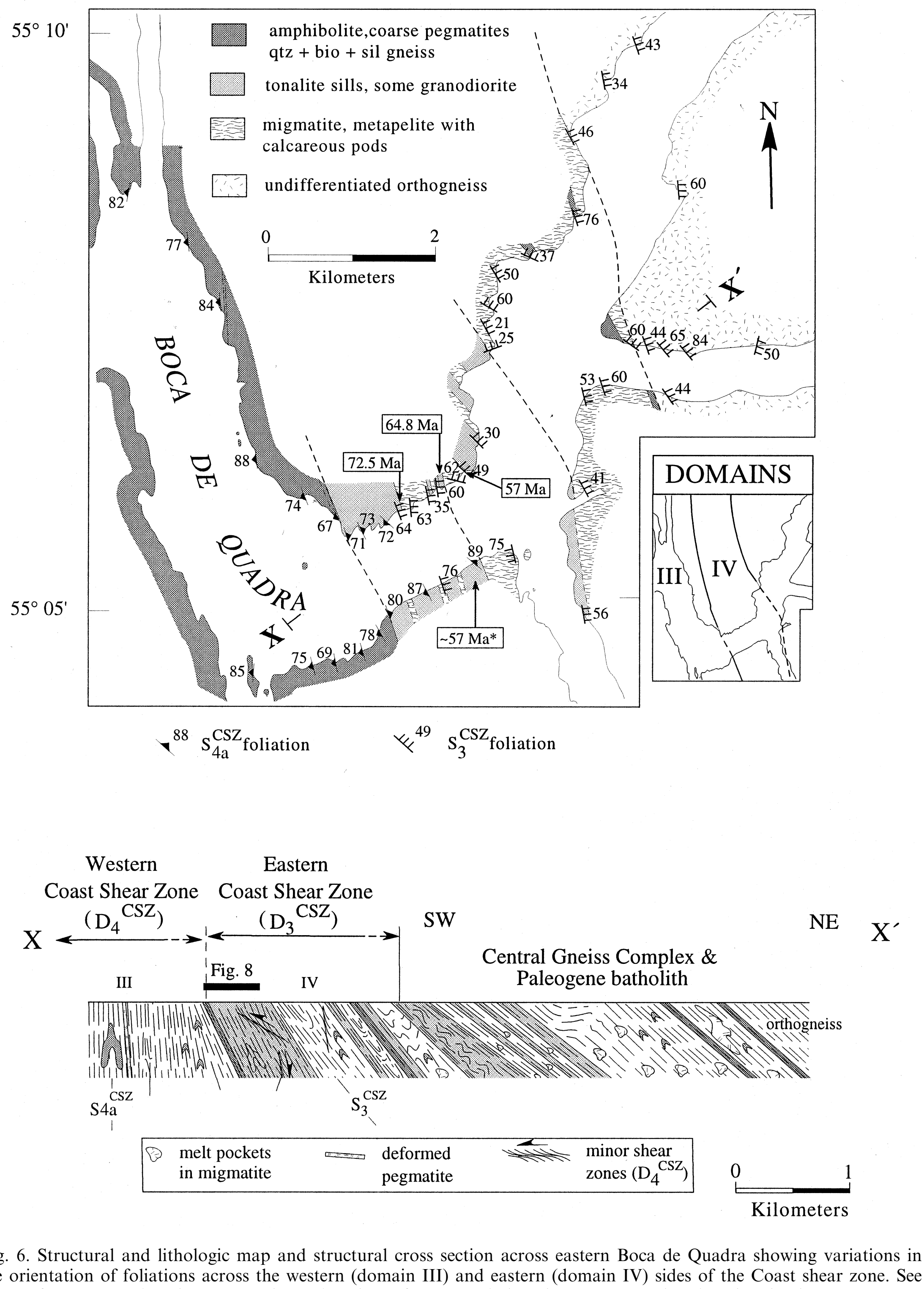

Fig. 6. Structural and lithologic map and structural cross section across eastern Boca de Quadra showing variations in the orientation of foliations across the western (domain III) and eastern (domain IV) sides of the Coast shear zone. See Fig. 1 for transect location. Inset shows location of structural domains. Cross section location is shown as X–X′. Foliation symbols are same as in Fig. 2. Boxed numbers refer to U–Pb isotopic dates from zircons. Ages are from this study (samples 94-200, 94-236 and 94-237) except asterisked age which is from Saleeby and Rubin (1989).

for the most part parallel intersection lineations, are formed by the intersection between S_3^{CSZ} and an older transposed foliation. In some localities S_3^{CSZ} is deformed by gently north-plunging, upright F_4^{CSZ} folds. Because these folds are most common near the boundary between domains III and IV, they are discussed below in the section on D_4^{CSZ} deformation patterns.

Mineral assemblages, cordierite paragenesis and textures

Within metasedimentary rocks of domain IV in eastern Sitklan Passage, a well exposed section (locality 93-145) of garnet + sillimanite + cordierite-bearing metapelites occurs adjacent to a deformed 65 Ma tonalite pluton. Here, S_3^{CSZ} comprised well-layered, granoblastic gneisses and schists interlayered with felsic orthogneisses, migmatites and amphibolite layers. Samples from this locality contain abundant sillimanite pseudomorphs of kyanite grains aligned parallel to L_3^{CSZ} on S_3^{CSZ} foliation planes and rare, highly resorbed and broken staurolite grains. Deformed garnet porphyroblasts contain relatively inclusion-free cores and rims that contain inclusions of non-aligned coarse-grained prismatic sillimanite (Fig. 7). This occurrence of sillimanite inclusions in garnet rims represents an initial phase of sillimanite growth (sil_1). Strongly aligned sillimanite in the matrix, including the sillimanite pseudomorphs of kyanite and sillimanite grains that are bent into parallelism with L_3^{CSZ} in pressure shadows of garnets represents a second phase of coarse-grained sillimanite growth (sil_2).

Deformed garnet porphyroblasts at locality 93-145 display coronas of recrystallized cordierite that are drawn out into strain shadows behind garnets (Fig. 7). The cordierite coronas form semicontinuous rims between garnet and sillimanite (sil_2), biotite and feldspar. Some minor symplectitic intergrowths of cordierite with quartz also occur. These textural relationships between garnet, sillimanite (both sil_1 and sil_2) and cordierite, and observations of embayed, irregular margins on garnet in contact with cordierite (Fig. 7) strongly suggest that the cordierite coronas were produced by a garnet-consuming reaction involving both sillimanite and quartz (2 grt + 5q + 4sil = 3 crd). In support of this interpretation, five core-to-rim step scans across garnets displaying cordierite coronas (see Table 2) yielded mineral chemistry that shows the following trends: (1) garnets are mostly very homogeneous in composition except at rims in contact with cordierite and (2) garnet rims in contact with cordierite show

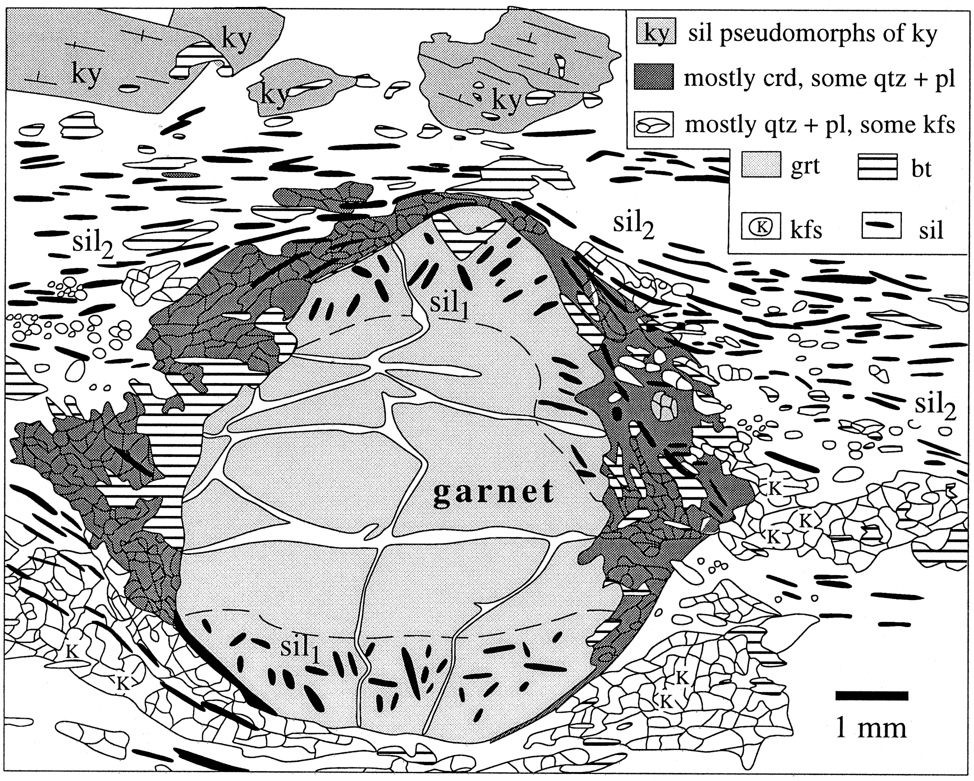

Fig. 7. Sketch showing metamorphic textures in a sample from locality 93-145 in the eastern Coast shear zone (domain IV) of Sitklan Passage containing the assemblage grt + sil + crd + qtz + kfs + bt + pl. Note corona of cordierite around garnet porphyroblast. Sil_1 (located in rim of garnet) and sil_2 (located in matrix) refer to two generations of sillimanite growth discussed in the text. The foliation parallel to the length of the sketch is S_3^{CSZ}. View is perpendicular to foliation and parallel to lineation ($L_{3\,m}^{CSZ}$). Sample was used in calulation of P–T conditions during the D_3^{CSZ} event of the eastern Coast shear zone and as evidence for a decompression reaction involving the production of cordierite at the expense of garnet and sillimanite (see Fig. 8). See text for discussion of textures and mineral assemblage.

moderate decreases in Mg, moderate increases in Fe, slight increases in Mn and very slight decreases in Ca. Similar trends also are observed and documented by Hollister (1977) and Selverstone and Hollister (1980) for rocks located in equivalent portions of the Central Gneiss complex east of the Coast shear zone near the Skeena River. As in these previous works, we interpret these mineral chemistry trends within garnets in contact with cordierite as indicating that Mg is partially incorporated into cordierite relative to garnet with a back diffusion of Mn into the remaining garnet (Selverstone and Hollister, 1980). The textural relationships we describe and the alignment of the minerals within S_3^{CSZ} also strongly suggest that cordierite formed prior to and/or during D_3^{CSZ} deformation in the eastern Coast shear zone.

Conditions of metamorphism, evidence for decompression and east-side-up displacement

Mineral chemistry of the major phases in samples from locality 93-145 (e.g. Fig. 7) and textural relationships involving the assemblage grt + sil + crd + qtz + mcr + bt + pl (Fig. 7) allow us to calculate the pressure–temperature conditions of metamorphism during or before D_3^{CSZ} deformation in the eastern Coast shear zone. Microprobe analyses (representative analyses in Table 2) were obtained using Cameca SX50 machines located at Virginia Polytechnic Institute and Princeton University. The samples contained no muscovite or chlorite, indicating that the rocks have not been affected by rehydration and retrogression.

Conditions of metamorphism for sample 93-145 (Fig. 8) were calculated using TWQ version 2.02 (Berman, 1991) and thermodynamic data from Berman (1988), Berman and Aranovich (1998), Aranovich and Berman (1996) and Berman *et al.* (1995). Non-ideal Ca–Na–K interactions are given by Fuhrman and Lindsley (1988) and the position of the staurolite-out reaction curve (Fig. 8) is from Holdaway *et al.* (1995). We use the TWQ program to calculate *P*–*T* conditions of stable curves for all possible reactions among the minerals present in the rock (Fig. 8). If the minerals are in equilibrium and the correct thermodynamic data are used, the calculated curves should intersect at a point. Our data for the intersections of the solid–solid reactions, which are not sensitive to water activity, result in a small scatter of intersection points. The average intersection for the equilibria thus derived suggests the metamorphic conditions for this sample were: $P = 5.6 \pm 0.4$ kbars and $T = 710 \pm 30°C$ (shaded oval in Fig. 8). These inferred pressure–temperature conditions agree well with the observed presence of sillimanite pseudomorphs of kyanite and staurolite in the sample. Using these *P*–*T* values we obtained an estimate of the activity of water (a_{H_2O}) for the rock of 0.75. This estimate was obtained by adjusting a_{H_2O} for dehydration reactions until the curves for those reactions passed through the area of the intersections (shaded area in Fig. 8) of the solid–solid reaction curves for the sample. We used this water activity to plot the positions of the dehydration curves shown in Fig. 8.

The sillimanite pseudomorphs after kyanite and staurolite in this sample suggest that the observed metamorphic assemblage represents a point along a *P*–*T* path from higher pressure and lower temperature conditions toward lower pressures and slightly higher temperatures. Kyanite and staurolite assemblages that characterize the rocks of the western thrust belt west of the Coast shear zone formed at 8–9 kbar (Crawford *et al.*, 1979). We assume that the kyanite and staurolite in this sample, now represented by the pseudomorphs, originally formed at similar high-pressure conditions. The breakdown of staurolite by the reaction st + q = alm + sil + water (curve 4 in Fig. 8) documents a temperature. This reaction explains the observed concentration of sillimanite inclusions in the outer rim zones of the garnet grains (Fig. 7).

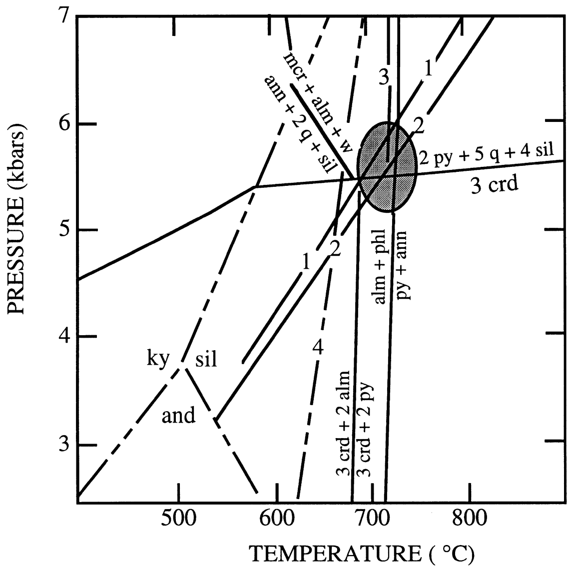

Fig. 8. Pressure–temperature diagram showing the metamorphic conditions for rocks affected by the D_3^{CSZ} event of the eastern Coast shear zone using mineral chemistry and textural data from Sitklan Passage (sample shown in Fig. 7). The average intersection of reaction curves for the equilibria in sample 93-145 (shaded oval region) is 5.6 ± 0.4 kbars, $710 \pm 30°C$. Not all the curves used in calculating this average intersection are shown for purposes of clarity. Solid line curves were calculated using mineral compositions using TWQ version 2.02 (Berman, 1991); dashed curves are additional mineral equilibria included for reference. For the reaction curves labeled on the diagram, py is pyrope, q is quartz, sil is sillimanite, crd is cordierite, fcrd is iron cordierite, gr is grossular, mcr is microcline, alm is almandine, w is water, an is anorthite, ann is annite, phl is phlogopite, ky is kyanite, and is andalusite. Numbered reaction curves are (1) 2alm + 5q + 4sil = 3fcrd, (2) 2sil + q + gr = 3An, (3) mcr + py + w = phl + 2q + sil, (4) st + q = alm + sil + w. Curve 4 is calculated for pure Fe staurolite and thus indicates the maximum temperature for staurolite stability. Mineral analyses used in this calculation are shown in Table 2. See text for discussion. Note the addition of f to crd in reaction 1 (the Fe end member reaction.)

Additional evidence for decompression during or slightly before formation of the S_3^{CSZ} foliation is the presence of cordierite replacing garnet in the pressure shadows around the garnet grains. This latter reaction provides the main constraints for the calculated pressure–temperature estimates for this sample. The low slope of the reaction producing cordierite at the expense of garnet and sillimanite with cordierite on the low-pressure side makes this reaction an excellent indicator of decompression. Hollister (1977, 1982) and Selverstone and Hollister (1980) calculated similar *P–T* conditions for a cordierite producing reaction during decompression for samples east of the Coast shear zone near the Skeena River. Our main additional contribution to this observation is that (1) we observe the production of cordierite during and/or before the formation of the S_3^{CSZ} foliation and (2) this reaction is consistent with decompression during D_3^{CSZ} in the eastern Coast shear zone. Evidence of decompression supports our interpretation of east-side-up, top-to-the-southwest displacement for D_3^{CSZ} deformation based on sense of shear indicators viewed parallel to down-dip stretching directions (L_3^{CSZ}). These form part of the S_3^{CSZ} foliation in domain IV and include asymmetric boudinage of amphibolite layers between metapelitic layers, C' shear bands and asymmetric tails of garnet porphyroblasts in metapelites.

THE WESTERN COAST SHEAR ZONE (D_4^{CSZ})

D_4^{CSZ} *fabric elements*

Between Portland Inlet and North Behm Canal, a steep, 1–2 km wide, zone of intensely developed, steeply-dipping *L–S* tectonites lies between the less steeply dipping foliations of structural domains II and IV (Figs 2 & 3). Deformation that produced the steep foliation of domain III constitutes the D_4^{CSZ} event of the western Coast shear zone. We recognize two types of foliations (S_{4a}^{CSZ} and S_{4b}^{CSZ}) and two distinctive styles of folds (F_{4a}^{CSZ} and F_{4b}^{CSZ}) within domain III (Fig. 9). The first, and dominant, foliation (S_{4a}^{CSZ}) is a preferred shape orientation of lenticular mineral aggregates and aligned biotite, hornblende and sillimanite minerals. On S_{4a}^{CSZ} foliation planes are steeply-plunging to subvertical mineral lineations ($L_{4\,m}^{CSZ}$, Fig. 3) defined by fibrolitic to coarse-grained, prismatic sillimanite in meta-pelitic layers, elongate quartz–biotite strain shadows on garnet porphyroblasts and coarse-grained hornblende in amphibolite layers. Abundant boudinage (e.g. Fig. 5f) parallel to the $L_{4\,m}^{CSZ}$ lineation indicates that this direction is a true stretching direction.

The first set of folds in domain III (F_{4a}^{CSZ}) are steeply to moderately north- and south-plunging folds of an older foliation that may represent either S_2^{WTB} or S_3^{CSZ}. S_{4a}^{CSZ} is aligned with the axial plane of the F_{4a}^{CSZ} folds, suggesting that these two structures probably formed together. $L_{4\,m}^{CSZ}$ everywhere exactly parallels both the axes of F_{4a}^{CSZ} folds and L_{4i}^{CSZ} intersection lineations. The latter are generated by intersections between S_{4a}^{CSZ} and older transposed foliations (S_2^{WTB} and S_3^{CSZ}, Fig. 3). This parallelism of fold axes and lineations contrasts with the oblique fold-lineation relationships that occur in domain II (Fig. 3).

The second style of folds (F_{4b}^{CSZ}) that occurs within and near the boundaries of domain III are tight to open asymmetric folds of S_{4a}^{CSZ} (Fig. 9). We have not delineated these folds as a distinct deformational event because, as discussed later, the development of these folds is consistent with progressive D_4^{CSZ} deformation within domain III. F_{4b}^{CSZ} folds display variable plunges to the north and south within a plane that is approximately parallel to or at a low angle to S_{4a}^{CSZ} (Fig. 10). They are consistently upright with moderately north-east-dipping axial planes and are non-coaxial with F_{4a}^{CSZ} folds. Parallel to the axial planes of F_{4b}^{CSZ} folds is a crenulation cleavage (S_{4b}^{CSZ}) defined by bent hornblende grains in amphibolite layers. This cleavage and their associated folds only occur within high strain zones in domain III and the eastern side of domain IV.

Textural relationships

Rocks in Boca de Quadra show textures that suggest sillimanite crystallized from the breakdown of kyanite and staurolite during formation of $L_{4\,m}^{CSZ}$–S_{4a}^{CSZ} tectonites. Strongly deformed and resorbed kyanite and staurolite grains mantle synkinematically deformed garnet porphyroblasts that display S-shaped patterns of quartz inclusion trails. Sillimanite mats pseudomorph kyanite in the matrix and form large (up to 2 cm long) symmetric strain shadows aligned subvertically around these garnets, parallel to $L_{4\,m}^{CSZ}$.

Grain refinement in micaceous quartzite and quartzo-feldspathic layers involved dynamic recrystallization of older phases. Larger grain sizes of quartz in strain shadows around surviving megacrysts of garnet compared to matrix grains suggests a reduction of grain size in these rocks by crystal-plastic processes. Nevertheless, quartz in the matrix is still generally much coarser than grains observed in domain II. Matrix quartz contains abundant polygonal subgrains with 120° grain boundaries and much less evidence of sutured grain boundaries than we observe in domain II, suggesting that most of these grains experienced almost full strain recovery. This assemblage and textures reflect a strong regional temperature gradient from west to east across the western Coast shear zone. Hollister (1982), Wood *et al.* (1991) and Crawford *et al.* (1991) document a similar eastward increase in temperature south of Portland Inlet. Subsequent retrogression of the high temperature assemblages on the west side of domain III resulted in muscovite, chlorite and

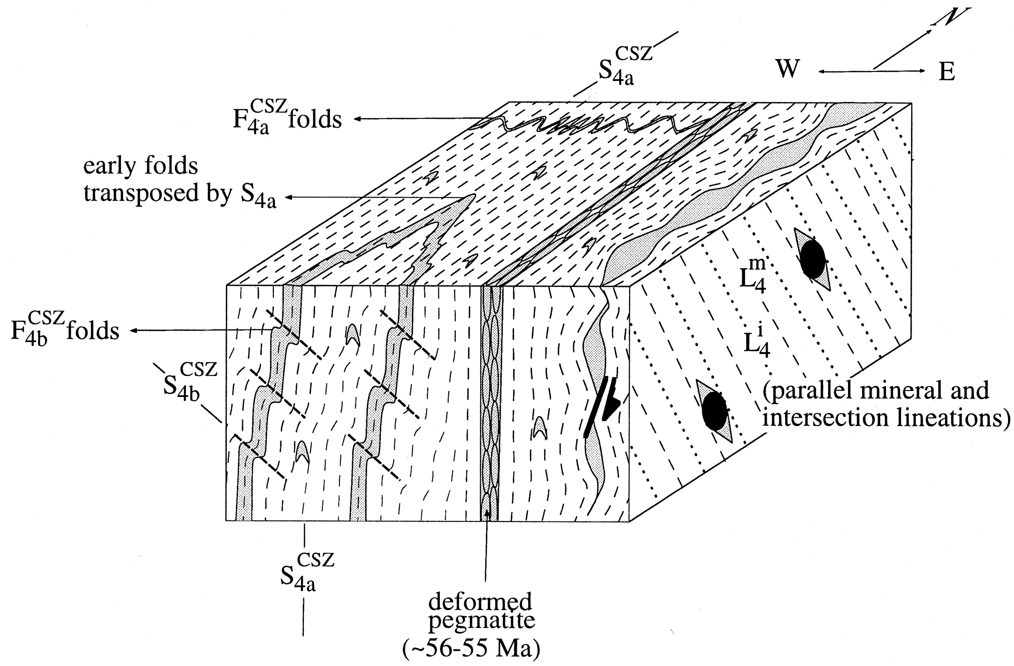

Fig. 9. Block sketch summarizing the main D_{4a}^{CSZ} and D_{4b}^{CSZ} fabric elements of the western Coast shear zone (domain III). Note dominant steeply-dipping to subvertical S_{4a}^{CSZ} foliation, steeply-plunging sillimanite and hornblende mineral lineations ($L_{4\,m}^{CSZ}$) and parallel intersection lineations (L_{4i}^{CSZ}), F_{4a}^{CSZ} folds of amphibolite layers (shaded), F_{4b}^{CSZ} folds of the S_{4a}^{CSZ} foliation and a S_{4b}^{CSZ} crenulation cleavage paralleling F_{4b}^{CSZ} axial planes. S_{4a}^{CSZ} affects the ~56–55 Ma pegmatite.

biotite rims around strongly deformed and resorbed garnets.

Boundaries of the western Coast shear zone

The westernmost boundary of the western Coast shear zone is defined by the following features that occur within less than 0.5 km of one another: (1) A reorientation and transposition of the D_{1-2}^{WTB} structures of domain II into a steep to sub-vertical orientation by D_4^{CSZ} in domain III. (2) The occurrence of down-dip sillimanite and hornblende mineral lineations on steeply-dipping S_{4a}^{CSZ} planes. (3) The occurrence of S_{4b}^{CSZ} and F_{4b}^{CSZ} structures. (4) The occurrence of undeformed to weakly deformed trondhjemite pegmatites that share the S_{4a}^{CSZ} foliation at their edges. These pegmatites become progressively more deformed and rotated into parallelism with S_{4a}^{CSZ} toward the center of domain III (compare Fig. 5d with Fig. 5e). In some localities the pegmatites are protomylonitic. Contrastingly, at the Coast shear zone western boundary, pegmatites are weakly deformed and highly discordant to the dominant S_2^{CSZ} foliation (Fig. 5d). (5) An abrupt change in fold axis–mineral lineation relationships from obliquely intersecting in domain II (F_2^{WTB}–$L_{2\,m}^{WTB}$, Fig. 3) to parallel in domain III (F_{4a}^{CSZ}–$L_{4\,m}^{CSZ}$, Fig. 3). These structural features reflect an apparent eastward increase in finite strain that is probably related to an eastward increase in the temperature of deformation in country rock across the transects. We place the eastern boundary of the western Coast shear zone at the eastern edge of dominantly solid-state deformed tonalite plutons. This eastern boundary displays a similar steepening and transposition of fabrics as the western boundary. Pegmatites that are strongly discordant with, and crosscut, S_3^{CSZ} also become progressively reoriented and more intensely deformed from east to west toward the center of domain III.

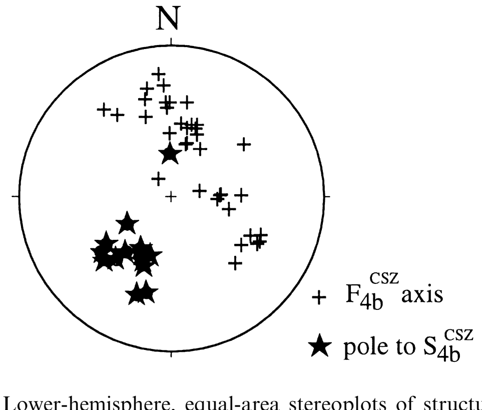

Fig. 10. Lower-hemisphere, equal-area stereoplots of structural data from domain III, western Coast shear zone. Poles to the S_{4b}^{CSZ} crenulation cleavage (stars) and F_{4b}^{CSZ} fold axes (crosses) are shown. See text for discussion.

Evidence for east-side-down displacement during D_4^{CSZ}

A range of different types of sense-of-shear indicators occur within domain III of the western Coast shear zone. All indicate bulk east-side-down motion during D_4^{CSZ} deformation. The first indicators are steeply dipping to sub-vertical minor shear zones that occur near the eastern boundary between domains III and IV (Figs 5g & 11). These shear zones represent areas of high D_4^{CSZ} strain. S_3^{CSZ} is visible in low strain areas between the high strain zones where it is overprinted and transposed to subvertical parallel to S_{4a}^{CSZ} (Fig. 11). An east-side-down sense of motion parallel to a $L_{4\,m}^{CSZ}$ lineation within the D_4^{CSZ} shear zones is indicated by the deflection of the S_3^{CSZ} foliation into high strain zones, C' shear bands and asymmetric tails (both sigma and delta types) on feldspar porphyroblasts (e.g. Fig. 5g). At the regional scale, the S_{4a}^{CSZ} foliation of the western Coast shear zone, shows a matching development and rotation of older foliations into the center of domain III. Near the center of domain III, asymmetric boudins (Figs 5f & 11) and C' shear bands indicate east-side-down shear parallel to L_{4a}^{CSZ}. Asymmetric tails on garnet and feldspar grains viewed parallel to L_{4a}^{CSZ} also suggest east-side-down shear senses although some west-down shear senses are also visible.

An analysis of F_{4b}^{CSZ} and S_{4b}^{CSZ} structures affecting the main S_{4a}^{CSZ} foliation in domain III also suggests east-side-down motion during D_4^{CSZ}. The following observations are used to model the progressive development of F_{4b}^{CSZ} and S_{4b}^{CSZ}. (1) The folds are associated with steeply-dipping, minor D_4^{CSZ} shear zones that display east-side down senses of motion parallel to $L_{4\,m}^{CSZ}$ and shear out the F_{4b}^{CSZ} fold limbs (Fig. 12a & b). (2) S_{4b}^{CSZ} is an asymmetric crenulation cleavage that is restricted to gently-dipping F_{4b}^{CSZ} fold limbs and has only been found in high D_4^{CSZ} strain zones. (3) Conjugate sets of crenulations do not develop and S_{4b}^{CSZ} does not occur on steeply dipping F_{4b}^{CSZ} fold limbs. (4) S_{4b}^{CSZ} forms a high angle with respect to S_{4a}^{CSZ} planes ($>45°$to $\sim85°$) and is penetrative with sharp boundaries. (5) S_{4b}^{CSZ} also shows varying degrees of development, becoming more penetrative as it aligns with S_{4a}^{CSZ}. The work of Price and Cosgrove (1990) and Jiang and White (1995) suggests that the development of this type of cleavage is related to contraction initiated at a high angle to a strong anisotropy formed by a pre-existing (in this case S_{4a}^{CSZ}) foliation.

Price and Cosgrove (1990, p. 488) have described a shear couple model that explains the relationships between S_{4b}^{CSZ} and F_{4b}^{CSZ} and observations of east-side-down shear zones that shear out limbs of F_{4b}^{CSZ} folds. We adapt this model as follows: during F_{4b}^{CSZ} folding, one limb of the asymmetric fold rotated into approximate parallelism with the direction of maximum instantaneous contraction and the other near normal to it. The limb oriented at a high angle to the direction of maximum instantaneous shortening preferentially formed the S_{4b}^{CSZ} crenulation cleavage which then tracks the rotation of the fold. The asymmetry of the S_{4b}^{CSZ} cleavage and discrete east-side-down shear planes that offset fold limbs confirm an east-side-down shear sense during F_{4b}^{CSZ} fold development (Fig. 12d).

A final indication of east-side-down shear sense during D_4^{CSZ} is a regional-scale progressive rotation of F_{4b}^{CSZ} axial planes into the sub-vertical plane of S_{4a}^{CSZ} with increasing fold tightness across domains III and eastern domain IV. Along Boca de Quadra, open F_{4b}^{CSZ} chevron folds display moderately east-dipping axial planes and steeply east-plunging sillimanite lineations. Further west near domain III, F_{4b}^{CSZ} folds are tighter and fold axial planes are much more steeply dipping to the east and northeast. The progressive change from larger angles (up to 47°) between S_{4a}^{CSZ} and F_{4b}^{CSZ} axial planes in domain IV to small angles

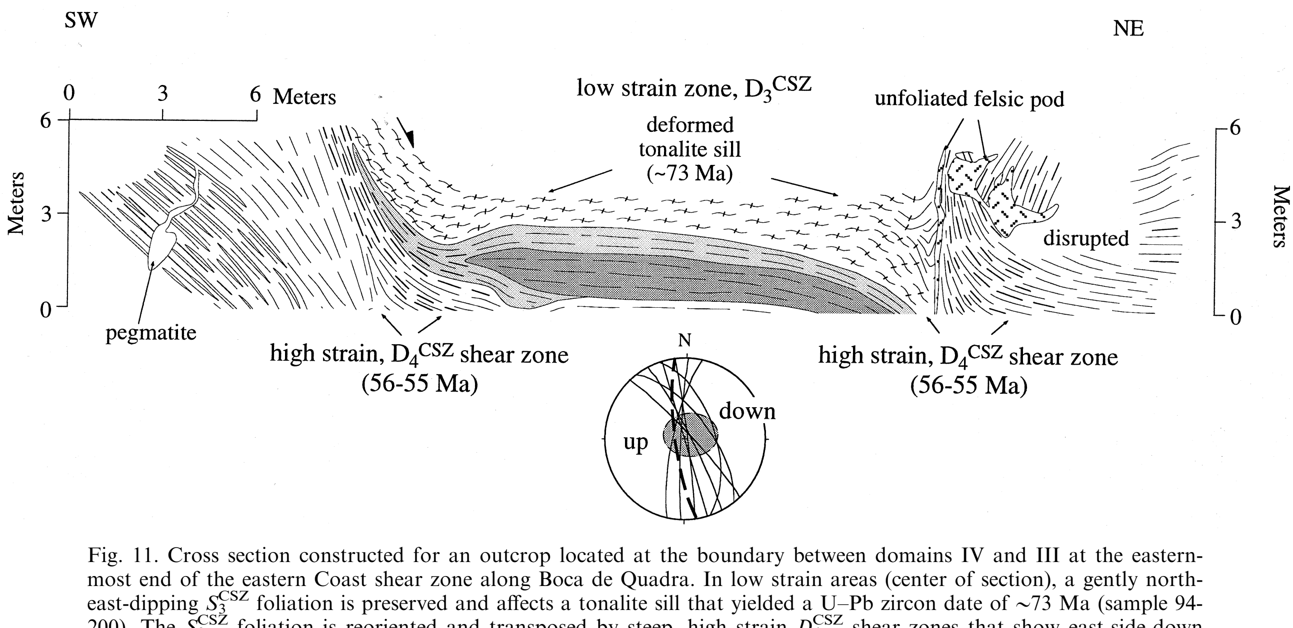

Fig. 11. Cross section constructed for an outcrop located at the boundary between domains IV and III at the easternmost end of the eastern Coast shear zone along Boca de Quadra. In low strain areas (center of section), a gently northeast-dipping S_3^{CSZ} foliation is preserved and affects a tonalite sill that yielded a U–Pb zircon date of ~73 Ma (sample 94-200). The S_3^{CSZ} foliation is reoriented and transposed by steep, high strain D_4^{CSZ} shear zones that show east-side-down shear senses. The lower-hemisphere, equal-area stereoplot shows the orientation of D_4^{CSZ} shear zones measured near the boundary between domains III and IV. The dashed circle on the stereoplot outlines the orientations of steeply-plunging stretching directions measured in these shear zones.

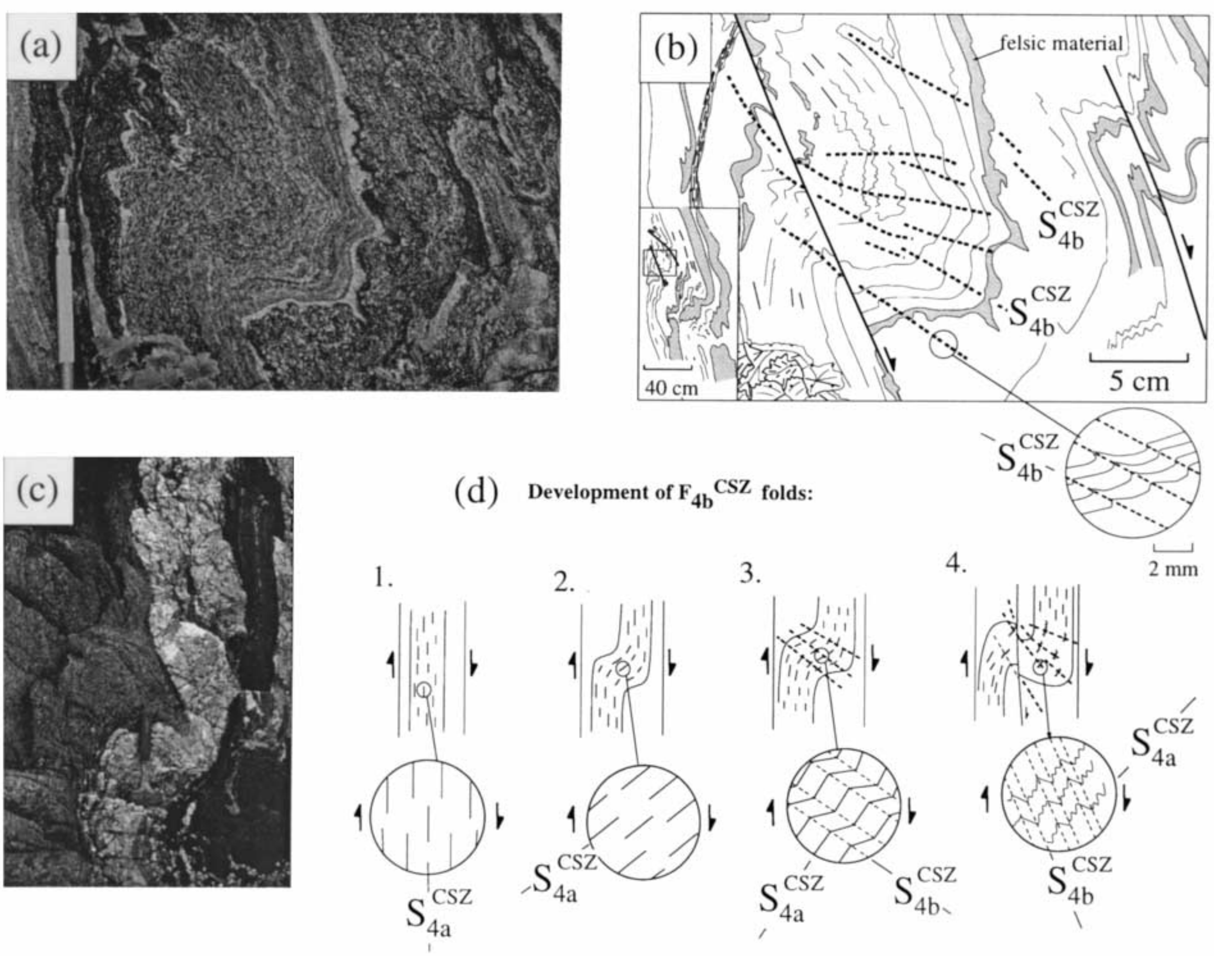

Fig. 12. Photograph (a) and interpretation (b) of F_{4b}^{CSZ}minor folds and S_{4b}^{CSZ} crenulation cleavage of the Coast shear zone (domain III). (c) Shows F_{4b}^{CSZ} folds affect pegmatites with interpreted ages of ~57–55 Ma. (d) East-side-down displacement during D_4^{CSZ} explains the development of F_{4b}^{CSZ} and S_{4b}^{CSZ} structures (modified from Price and Cosgrove, 1990).

(~0–27°) in domain III suggests an east-side-down rotation of fold axial planes toward S_{4a}^{CSZ} orientations.

AGE OF DEFORMATION EVENTS

D_{1-2}^{WTB} *deformation*

By association with mid-Cretaceous plutonism (Cook *et al.*, 1991; Rubin and Saleeby, 1992; McClelland *et al.*, 1992), a regional correlation of distinctive high *P–T* kyanite-grade metamorphic assemblages, and west- to southwest-directed thrust faults across the western thrust belt suggests that D_{1-2}^{WTB} features in domains Ia, Ib and II are mid-Cretaceous (100–90 Ma) or older. In support of this view, we observe at the eastern end of domain II a weakly deformed pegmatite (sample 94-31, Sitklan Passage) oriented discordantly with respect to the main S_2^{WTB} foliation. Zircons collected from this sample are very clear with few inclusions and fractures; most are colorless, small (< 145 m) bipyramidal rods with from 6:1 to 8:1 elongation. Five fractions of variable size were analyzed using standard isotope dilution techniques and thermal ionization mass spectrometry (Table 1) (Gehrels *et al.*, 1991). All yielded concordant ages (Fig. 13a). We interpret the crystallization age as 92 ± 2 Ma. The high discordance and weak state of deformation exhibited by this pegmatite suggests that much of D_{1-2}^{WTB} predates ~92 Ma.

D_3^{CSZ} *and* D_4^{CSZ} *deformation*

Within structural domain IV, we collected and dated zircons from several tonalite and granodioritic intrusives that display key structural relationships with respect to the S_3^{CSZ} foliation. Within a low D_4^{CSZ} strain zone in domain IV of Boca de Quadra, we dated an intensely solid-state deformed tonalite intrusive sill (sample 94-200) that shares the northeast-dipping S_3^{CSZ} foliation of adjacent country rock (Fig. 11). This sample yielded zircons that are generally yellowish-orange in color, free of inclusions, and not highly elongate. Broken and fractured grains are common. Five size fractions were analyzed, all of which are analytically concordant at 72.5 ± 1.0 Ma (Fig. 13b).

Other tonalite intrusives collected from domain IV along Boca de Quadra (sample 94-236) and Sitklan

Passage (samples 94-33) yielded zircons with interpreted ages close to 65 Ma. Sample 94-236 yielded a large number of zircon grains, which have a wide range of colors (colorless, yellow, tan) and shape (stubby to highly elongate). Most grains have abundant inclusions. Four fractions of variable size yielded concordant analyses, with an age of 64.8 ± 0.8 Ma (Fig. 13c). Zircons in sample 94-33 (Fig. 13d) are slightly pinkish or tan in color and not highly elongate (generally from 2:1 to 3:1). Dark inclusions are abundant in most grains. Six size fractions were analyzed, of which five are analytically concordant and indistinguishable. These grains yield an interpreted age of 65 ± 1 Ma. A sixth grain yields slightly older U–Pb ages, presumably due to the presence of a small inherited component.

Both samples 94-33 and 94-236 are from plutons that are affected by the dominant S_3^{CSZ} foliation in domain IV. Near the western boundary of domain IV sample 94-236 is cut by minor D_4^{CSZ} shear zones. In some localities within the interiors of these plutons aligned hornblende and tabular plagioclase grains, and little evidence of dynamic recrystallization in quartz and plagioclase provide evidence of a magmatic flow foliation. These relationships indicate that these plutons intruded prior to or during D_3^{CSZ} and prior to D_4^{CSZ}. As such the dates from these plutons give us a ~65 Ma lower limit on the age of D_3^{CSZ}.

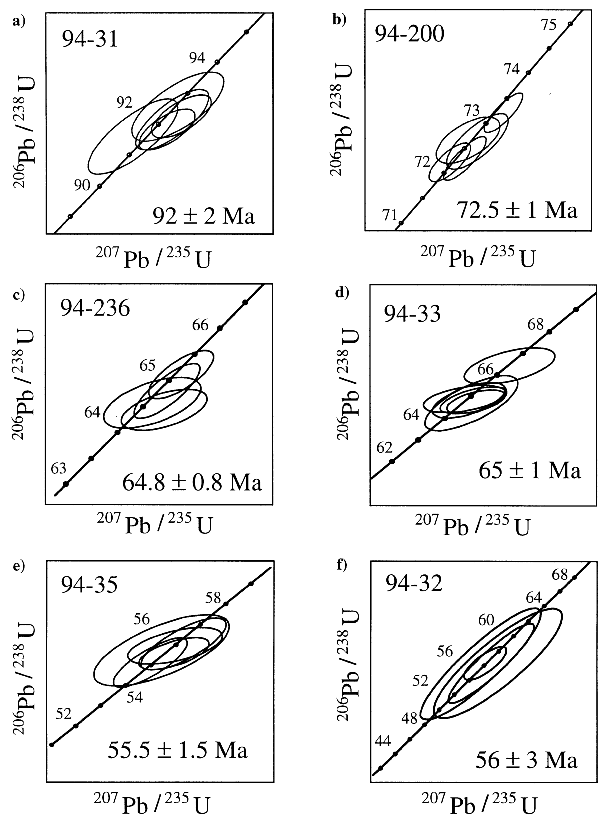

Fig. 13. U–Pb concordia plots of zircon fractions from six intrusive samples collected along Sitklan Passage and Boca de Quadra. (a) Sample 94-31 from western Sitklan Passage, (b) sample 94-236 from Boca de Quadra, (c) sample 94-33 from western Sitklan Passage, (d) sample 94-200 from low strain zone in Boca de Quadra, (e) sample 94-32 from Sitklan Passage, (f) sample 94-35 from Sitklan Passage. See Figs 1–3 for sample locations. Interpreted ages shown in lower right corners of plots. Tabulated data and analysis parameters are shown in Table 1. See text for discussion.

At the eastern edge of domain IV, an undeformed tonalite pluton exposed in eastern Sitklan Passage (sample 94-35) crosscuts the S_3^{CSZ} foliation. This sample yielded a large quantity of zircons that are slightly pinkish or tan in color and highly translucent. Most grains have few inclusions and are moderately elongate (from 3:1 to 5:1). The five size fractions analyzed are all concordant and yield an interpreted age of 55.5 ± 1.5 Ma (Fig. 13e). This age places an upper limit on the duration of D_3^{CSZ} deformation. In support of this upper limit, a pluton from domain IV that is unaffected by D_4^{CSZ} and crosscuts D_3^{CSZ} in Boca de Quadra (sample 94-237) yielded a crystallization age of 57.0 ± 3 Ma based on three concordant grains (Table 1). This sample contained a small number of grains that ranged from clear and colorless to tan/brown and cloudy. We analyzed 12 fractions of variable size. However, because most grains from this sample contain inherited components with an average of ~181 Ma we omit this sample from our presentation.

Near the boundaries of the steep western zone of the Coast shear zone (domain III) are numerous weakly deformed swarms of trondhjemitic pegmatites. These pegmatites are part of the swarm that marks the western limit of a Tertiary intrusive complex (Paleogene batholith) of dominantly tonalitic composition north of the Skeena River. In domain IV, along Sitklan Passage, strongly discordant pegmatites of this swarm cross-cut the S_3^{CSZ} foliation. These pegmatites also cross-cut the S_2^{WTB} of the western thrust belt. Toward the center of domain III, these pegmatites become progressively more intensely deformed into strong concordance with S_{4a}^{CSZ}.

At the easternmost side of domain III in Sitklan Passage (Fig. 2) we collected a representative pegmatite (sample 94-32) that cross-cuts the S_2^{WTB} foliation of domain II and weakly shares the S_{4a}^{CSZ} foliation of domain III. This sample yielded a small number of highly elongate (from 6:1 to 8:1) rods, most of which are generally colorless and free of inclusions and fractures. Seven size fractions from this sample were analyzed, five of which are apparently concordant at 56 ± 3 Ma; two grains have inherited components (Fig. 13f). Similar pegmatites dated at ~57–55 Ma by Saleeby and Rubin (1989) from within domain IV confirm our age determination for these pegmatites.

Together, our analyses indicate that D_3^{CSZ} of the eastern Coast shear zone occurred during the interval 65–57 Ma and D_4^{CSZ} of the western Coast shear zone occurred during the interval 57–55 Ma (Fig. 14). Supporting our interpretation for the western Coast shear zone, parts of the Quottoon pluton located

Table 1. U–Pb isotopic data and apparent ages

Grain characteristics		Weight (μg)	(pg)	Concentrations (ppm)	(ppm)	Pb isotopic ratios			Apparent ages		
Size	#		Pbc	Pb	U	206 m/204	06c/204	2 06/208	$^{206*}Pb/^{238}U$	$^{207*}Pb/^{235}U$	$^{207*}Pb/^{206*}Pb$
						94-200					
E	30	152	25	9.92	891	3950	6640	10.4	72.2 ± 0.3	72.1 ± 0.4	70 ± 9
A	8	151	30	4.84	417	1520	2260	7.9	72.7 ± 0.4	72.6 ± 0.7	70 ± 17
A	10	217	64	7.49	645	1600	1900	8.1	72.6 ± 0.5	72.8 ± 0.6	78 ± 13
D	25	185	40	10.41	930	3350	4470	10.4	72.3 ± 0.4	72.5 ± 0.4	79 ± 8
F	50	182	21	10.23	907	5550	10400	10.4	73.2 ± 0.3	73.4 ± 0.4	81 ± 7
						94-236					
E	30	239	51	3.13	281	865	1072	4.9	64.6 ± 0.4	64.7 ± 0.8	69 ± 24
C	15	315	34	2.93	275	1580	2230	6.4	65.1 ± 0.4	65.3 ± 0.5	70 ± 13
A	8	340	20	1.81	170	1840	3600	5.9	64.8 ± 0.4	64.9 ± 0.5	71 ± 12
A	8	364	70	4.21	383	925	1077	5.3	64.4 ± 0.3	64.9 ± 0.7	83 ± 22
						94-237					
A	1	32	14	5.81	652	2590	9770	17.5	60 ± 0.4	60 ± 0.5	60 ± 11
A	1	22	14	12.83	1490	5050	18700	18.4	58.2 ± 0.5	58.3 ± 0.5	62 ± 7
A	1	45	18	3.12	378	9720	12500	29.8	56.9 ± 0.7	57.3 ± 0.7	73 ± 8
A	1	33	14	2.81	308	9700	34250	32.9	63.1 ± 0.5	63.4 ± 0.7	73 ± 8
B	10	241	18	18.88	1460	17300	39400	11.4	84.3 ± 0.4	85.5 ± 0.5	118 ± 5
D	20	143	23	14.85	1174	6160	10900	16.4	84.7 ± 0.3	85.8 ± 0.4	118 ± 6
C	20	221	39	22.69	1640	8300	11170	10.8	89.6 ± 0.5	90.7 ± 0.5	120 ± 6
C	20	184	21	14.77	1000	8300	15560	12.6	97.1 ± 0.5	98.4 ± 0.5	130 ± 6
F	30	98	17	14.7	789	9650	23500	9.5	119.6 ± 0.5	121.5 ± 0.5	158 ± 6
A	1	60	85	13.44	554	548	620	4.6	135.1 ± 1.1	137 ± 2.4	170 ± 36
						94-31					
C	10	146	16	1.89	143	1250	3470	45.3	91.6 ± 0.9	91.1 ± 1.3	79 ± 21
G	30	138	32	2.17	151	624	896	16	92.6 ± 1.8	92.6 ± 1.4	95 ± 24
D	20	140	13	2.91	218	2220	10330	33.9	92.1 ± 0.8	92.4 ± 1.1	100 ± 18
C	20	205	14	4.33	330	4370	15600	77.8	91.8 ± 0.6	92.3 ± 0.8	103 ± 15
C	20	186	14	3.82	288	3800	13300	50.7	92.3 ± 0.6	92.8 ± 0.9	106 ± 16
						94-32					
B	8	116	13	0.97	10.8	150	538	12.6	56.2 ± 6.1	55.5 ± 7.3	28 ± 130
E	20	240	23	0.41	40.1	257	435	4.6	56.3 ± 1.8	56.2 ± 2.4	51 ± 62
D	15	160	10	0.21	26.4	254	5680	68.3	56.3 ± 4.3	56.9 ± 4.8	84 ± 79
G	40	138	18	0.22	20.8	117	228	6.2	56.3 ± 5.6	57.8 ± 6.9	123 ± 150

					94-33						
C	20	210	96	5.96	529	663	731	5.2	64.9 ± 0.5	64.7 ± 1.3	60 ± 44
F	40	136	26	2.42	222	759	1210	5.7	64.8 ± 0.6	64.9 ± 1.2	68 ± 34
A	8	231	64	2.78	244	602	710	5.5	66.4 ± 0.7	66.5 ± 1.5	68 ± 44
B	10	165	75	6.79	600	840	970	4.7	64.8 ± 0.5	65.1 ± 1.1	74 ± 32
B	10	154	18	13.54	1250	690	1520	5.9	64.7 ± 1.0	65 ± 1.4	76 ± 38
E	20	122	46	3.48	320	910	1160	5.7	64.8 ± 0.5	65.2 ± 0.8	80 ± 28
					94-35						
A	10	157	36	1.51	138	214	286	3.8	55.7 ± 1.4	55.4 ± 2.3	44 ± 72
E	30	117	18	1.45	161	605	1342	7.1	55.1 ± 0.9	54.9 ± 1.3	49 ± 32
B	8	142	43	1.16	116	350	447	4.8	55.9 ± 0.7	56 ± 1.6	58 ± 57
D	20	180	28	0.63	64	372	561	4.9	56 ± 1.1	56.3 ± 1.5	68 ± 39
E	20	95	48	2.28	228	382	475	4.8	55.6 ± 0.7	55.9 ± 1.2	71 ± 40
					94-36						
A	1	15	18	13.61	1250	690	1505	6.1	65.2 ± 1.0	65.4 ± 1.3	74 ± 29
F	30	90	30	10.39	877	2030	3050	10.5	76.4 ± 0.4	76.8 ± 0.6	90 ± 15
A	1	14	11	4.84	391	4300	43800	13.3	81.4 ± 0.5	82.5 ± 0.8	113 ± 16
A	1	20	15	19.8	1473	5200	15500	12.8	88.8 ± 0.6	90 ± 0.7	121 ± 11
B	10	180	32	9.03	741	3300	4780	12.8	80 ± 0.4	81.5 ± 0.6	124 ± 13
B	10	165	20	9.46	6.95	7200	14280	11.7	89.1 ± 0.4	92.3 ± 0.5	177 ± 7
D	20	140	19	3.35	276	1570	3190	12.1	78.9 ± 0.6	82.9 ± 0.9	201 ± 18
A	1	18	9	11.43	967	5300	12600	16.3	79 ± 0.6	83.3 ± 0.6	208 ± 10
E	30	168	16	3.43	275	2360	6190	13.1	82.1 ± 0.5	87.4 ± 0.8	233 ± 16
A	1	14	17	22.88	1085	2480	2820	5.84	126.6 ± 1.0	132.2 ± 1.2	234 ± 12
A	1	12	38	8.06	650	2130	2900	16.5	82.09 ± 0.5	88.3 ± 0.6	258 ± 13
A	1	17	24	52.01	1481	7800	13300	5.64	209.9 ± 1.5	218.3 ± 1.7	310 ± 8

* = radiogenic Pb.

Pbc = Total common Pb in picograms.

Grain size: A = 0.175 μm, B = 145–175 μm, C = 125–145 μm, D = 100–125 μm, E = 80–100 μm, F = 63–80 μm, G = 45–63 μm. 206 m/204 is measured ratio, uncorrected for blank, spike, fractionation, or initial Pb. 206c/204 and 206/208 are corrected for blank, spike, fractionation, or initial Pb. Pb and U concentrations have uncertainties of up to 25% due to uncertainty in grain weight. Constants used: 235 = 9.8485×10^{-10}, 238 = 1.55125×10^{-10}, 238/235 = 137.88. All uncertainties are at the 95% confidence level. Pb blank generally ranged from 2 to 10 pg. U blank was <1 pg. Isotope ratios are corrected for fractionation of 0.14 ± 0.40 for UO_2. Initial Pb composition interpreted from Stacey and Kramers (1975), with uncertainties of 1.0 for 206/204, 0.3 for 207/207, and 2.0 for 206/208. All analyses conducted using conventional isotope dilution and thermal ionization mass spectrometry as described by Gehrels *et al.* (1991).

Table 2. Representative microprobe analyses, and step scan (bottom) across garnet (rim on left) with cordierite corona

	Grt_r	Grt_c	Crd corona	pl	mrc	bt_a
SiO_2	37.96	38.19	47.08	59.56	64.40	34.80
TiO_2						4.98
Al_2O_3	22.29	22.32	32.73	26.25	18.99	18.31
FeO	34.52	31.35	7.68	0.70	0.05	17.66
MnO	1.79	1.58	0.13			0.03
MgO	4.96	6.45	9.07			10.16
CaO	1.38	1.46		7.45	0.03	
Na_2O				7.40	1.81	
K_2O				0.22	12.98	8.80
BaO				0.02	1.50	0.27
Total	102.90	101.35	96.70	101.60	100.21	95.01
Si	2.94	2.96	4.92	2.63	2.98	2.63
Ti						0.28
Al	2.04	2.04	4.04	1.36	1.03	1.63
Fe	2.24	2.04	0.67	0.03		1.12
Mn	0.12	0.10	0.01			
Mg	0.57	0.75	1.41			1.14
Ca	0.12	0.12		0.35		
Na				0.63	0.16	0.02
K				0.01	0.76	0.85
Ba					0.03	0.01
O, OH	12	12	18	8	8	12

r = rim, c = core, a = adjacent.

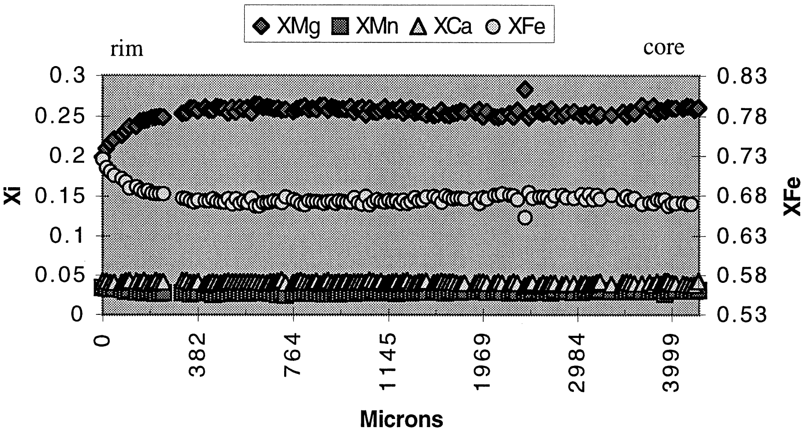

south of Portland Inlet (Fig. 1) yielded an age of 58.6 Ma (Gehrels *et al.*, 1991). This pluton is affected by steep solid-state, D_4^{CSZ} foliations at its western margin. Further east it is mostly undeformed and appears unaffected by D_3^{CSZ} structures. In central southeast Alaska, McClelland *et al.* (1992) report U–Pb dates from syntectonic and cross-cutting intrusives indicating that deformation within the Coast shear zone in general had evolved prior to 63.5 Ma, continued through ~59.5 Ma and had ceased by ~50 Ma.

DISCUSSION

Structural data, metamorphic mineral assemblages and textures, and U–Pb geochronologic data collected across five transects of the Coast shear zone north of Portland Inlet define a new two-stage (D_3^{CSZ} and D_4^{CSZ}) model for deformation in the Coast shear zone (Figs 14 & 15). D_3^{CSZ} dominates the eastern side of the Coast shear zone where the main foliation dips moderately to the north and northeast, and stretching lineations plunge northerly to easterly. D_3^{CSZ} involved east-side-up, top-to-the-southwest displacements between 65 Ma and ~57 Ma during emplacement of tonalitic and granodioritic plutons of the Coast Mountains Batholith. Within a narrower, 1–2 km wide, zone comprised of a steep to subvertical foliation on the western side of the Coast shear zone, D_4^{CSZ} deformation involved down-dip east-side-down motion between ~57 Ma and 55 Ma. D_4^{CSZ} in this narrow western zone, overprints, reorients and transposes both D_3^{CSZ} structures of the eastern Coast shear zone and pre-90 Ma D_{1-2}^{CSZ} structures of the mid-Cretaceous western thrust belt (Figs 14 & 15).

The two-stage history for the Coast shear zone described here both expands and significantly changes previously proposed single-phase styles of deformation for the Coast shear zone north of Portland Inlet. East-side-down displacement during D_4^{CSZ} differs with models involving east-side-up motion in the Coast shear zone and tilting of the batholith during the

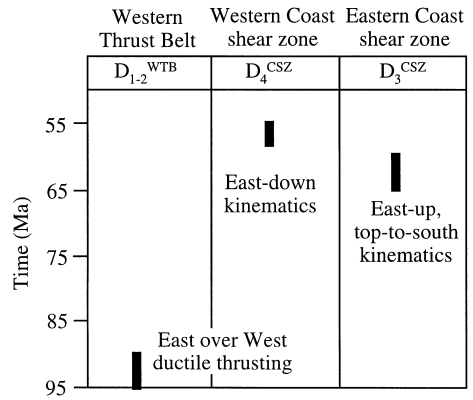

Fig. 14. Time–space diagram summarizing the spatial distribution of deformation events D_{1-2}^{WTB}, D_3^{CSZ}, and D_4^{CSZ} across the transects. Note division of the Coast shear zone into western and eastern sides, each of which preserves different styles and ages of fabrics.

Paleocene (Hollister, 1982; Crawford *et al.*, 1987; Ingram and Hutton, 1994). Nevertheless, it is consistent with the observations of McClelland *et al.* (1992) indicating a complex history of motion in the Petersburg segment of the Coast shear zone where deformation continued through ~59 Ma and terminated prior to 50 Ma.

Resolving the apparent discrepancy between previous models and our newly proposed two-stage model, we assert that the early east-side-up, top-to-the-southwest transport (D_3^{CSZ}) documented in this study for the interval 65–57 Ma is consistent with interpretations of reverse, east-side-up motion in the Coast shear zone proposed by Crawford *et al.* (1987), McClelland *et al.* (1992) and Ingram and Hutton (1994). In accordance with relationships reported in these older studies, our data indicate that east-side-up displacements during D_3^{CSZ} accompanied and, in some cases, outlasted the intrusion of numerous tabular plutons that thickened the crust during widespread batholith construction within and east of the Coast shear zone. Strain localization at the western margin of the batholith resulted in an abrupt change in structural level across the Coast shear zone with high-temperature, low-pressure migmatitic crust of the batholith to the east and the relatively colder, high-pressure rocks of the mid-Cretaceous western thrust belt to the west. Once developed, deformation could have facilitated the ascent and emplacement of large tabular plutons during east-side-up displacements within the eastern Coast shear zone (cf. Ingram and Hutton, 1994). The coincidence in location between the western boundary of the batholith and the location of the Coast shear zone is also consistent with suggestions that large strains within the Coast Mountains are associated with areas dominated by melt and/or plutons because of the low strength of these zones (Hollister and Crawford, 1986; Davidson *et al.*, 1992; Hollister, 1993).

East-side-down displacements during D_4^{CSZ} may reflect several processes that were occurring within the orogen during the Eocene and Paleocene. First, D_4^{CSZ} may be related to the collapse of an overthickened welt created by voluminous pluton emplacement, convergence and east-side-up displacements during D_3^{CSZ}. A similar explanation for deformation in the Coast shear zone was first proposed by McClelland *et al.* (1992) although their interpretation invoked the collapse of a crustal welt produced by mid-Cretaceous

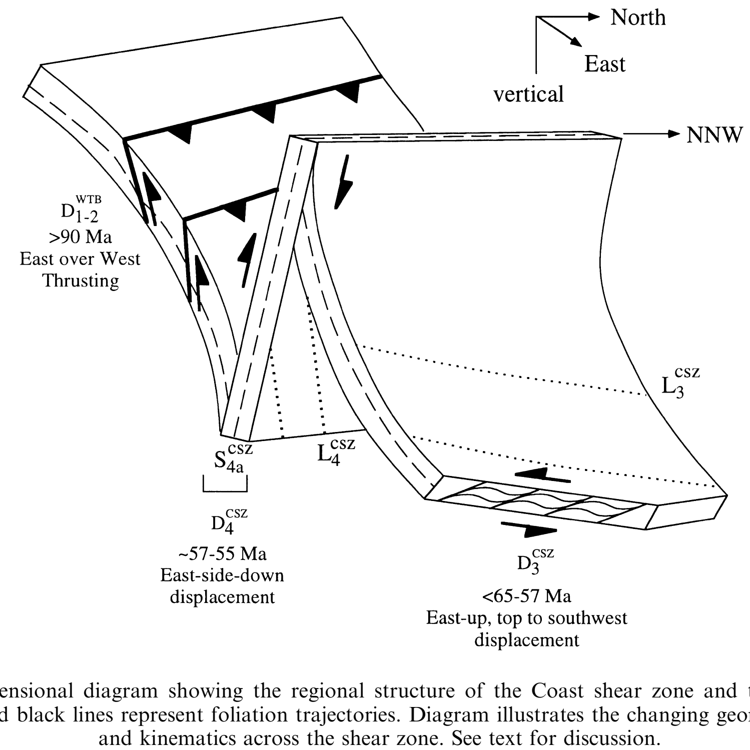

Fig. 15. Three-dimensional diagram showing the regional structure of the Coast shear zone and the adjacent crust it affects. Thin, curved black lines represent foliation trajectories. Diagram illustrates the changing geometry of fabrics, age and kinematics across the shear zone. See text for discussion.

thrusting and east-side-up tilting. This explanation implies that the Coast shear zone and batholith may record a final period of crustal readjustment and collapse following an earlier period of crustal thickening that accompanied construction of the batholith.

Alternatively, the two distinctive phases of deformation in the Coast shear zone may result from changes in mantle flow patterns and plate interactions during emplacement of the Coast Mountains batholith. Tobisch *et al.* (1995) describe fluctuating extensional and contractional strain patterns during emplacement of the Cretaceous Sierra Nevada batholith (Tobisch *et al.*, 1995). They proposed that mantle corner flow and a gradual change form orogen-normal convergence to orogen-parallel translation could lead to fluctuating strain fields that affect deformation patterns during batholith emplacement. A similar model where crustal relaxation and collapse of a welt are linked to changing plate conditions could also apply to the northern Coast Mountains although the angle of convergence and history of Kula plate motion is not well known (e.g. Sisson and Pavlis, 1993). It seems clear, at least, that the variable history of motion within the Coast shear zone reflects a changing response of the crust to different periods of batholith development along a convergent to obliquely-convergent margin.

Finally, with regard to strike-slip models for the Coast shear zone, we suggest that D_3^{CSZ} deformation in the eastern Coast shear zone may be kinematically compatible with structures interpreted to result from dextral transpressional east of the Coast shear zone near the Skeena River (Andronicos *et al.*, 1996). The east-side-up, top-to-the-southwest sense of motion results in a component of orogen parallel displacement during D_3^{CSZ} and may have formed concomitantly with zones interpreted as resulting from transpression in the Central Gneiss complex.

CONCLUSIONS

West of the Coast shear zone north of Portland Canal, deformation (D_{1-2}^{WTB}) produced penetrative S-tectonites, a tectonic imbrication of lithologically distinctive crustal fragments, and west to southwest-vergent thrust faults prior to 92 Ma. Thrust faults are marked by inverted metamorphic gradients, abrupt changes in fold and foliation geometries, and narrow, 10–15 m wide, zones that display east over west senses of displacement.

New structural, metamorphic and geochronologic data indicate that the western and eastern sides of the Coast shear zone record different structural styles, foliation orientations, senses of displacement and fabric ages. The western Coast shear zone is defined by a narrow, 1–2 km wide, high strain zone containing a steeply-dipping to subvertical foliation (S_4^{CSZ}) that overprints high-pressure (8–9 kbars) D_{1-2}^{WTB} structures of the western thrust belt. This foliation also affects ~59 Ma plutons at the western boundary of the Coast Mountains batholith south of Portland Inlet. S_{4a}^{CSZ} was produced during a phase of deformation (D_4^{CSZ}) that involved bulk east-side-down displacements parallel to a steeply-plunging, down-dip sillimanite and hornblende mineral lineation (L_4^{CSZ}) during the interval ~57–55 Ma. Other structures produced during D_4^{CSZ} include two styles of non-coaxial folds (F_{4a}^{CSZ} and F_{4b}^{CSZ}) and a crenulation cleavage (S_{4b}^{CSZ}) that parallels the axial planes of F_{4b}^{CSZ} folds.

The eastern side of the Coast shear zone contains a moderately to gently, north-northeast-dipping to east-dipping foliation (S_3^{CSZ}) and a gently to moderately north- and east-plunging mineral lineation. These structures were produced during deformation (D_3^{CSZ}) that involved east-side-up, top-to-the-southwest displacements between ~65 Ma and 57 Ma. Deformation during D_4^{CSZ}, reoriented and transposed S_3^{CSZ} into a subvertical orientation. Garnet + sillimanite + cordierite assemblages, and textural evidence indicating decompression of rocks equilibrating at 5.6 ± 0.4 kbars, 710 ± 30°C during or slightly prior to D_3^{CSZ} supports east-side-up displacement during D_3^{CSZ} prior to D_4^{CSZ}. D_3^{CSZ} corresponds to a period of widespread batholith construction by the syntectonic intrusion of numerous tabular plutons, crustal thickening by tectonic and magmatic processes, east-side-up tilting, and rapid exhumation of the deep-seated roots of the Coast Mountains batholith. D_4^{CSZ} east-side-down transport appears to represent a period of crustal relaxation and possibly tectonic collapse following a period of intense crustal thickening and pluton emplacement. This multistage displacement history appears to reflect a changing response of the crust to different periods of batholith development during overall convergence or oblique-convergence.

Acknowledgements—Research conducted for this study was supported by a National Science Foundation Postdoctoral Fellowship to K. A. Klepeis and a National Science Foundation grant to M. L. Crawford and G. E. Gehrels. We thank Lincoln Hollister, Cameron Davidson, Chris Andronicos and Dominique Chardon for helpful discussions and comments on deformation patterns in the Coast Mountains. K.A.K. thanks Bryn Mawr College and Princeton University for use of facilities during the data collection and reduction phase of this study. Thanks also go to Bill Crawford, Krishna Sinha, Hal Bosbyshell, Jennifer Lindline, Carol Simpson, and Mink Bay Lodge. Helpful reviews by H. Fossen and L. Kennedy greatly improved the original mansucript.

REFERENCES

Andronicos, C., Davidson, C. and Hollister, L. S. (1996) A dextral, orogen-parallel transcurrent shear zone at the eastern margin of the Quottoon pluton, Coast orogen, British Columbia. *Geological Society of America Abstracts with Programs* **28**, 651.

Aranovich, L. Y. and Berman, R. G. (1996) Optimized standard state and mixing properties of minerals: II. Comparisons, predictions and applications. *Contributions to Mineralogy and Petrology* **126**(1–2), 25–37.

Beck, M. E. Jr. (1989) Paleomagnetism of continental North America: Implications for displacement of crustal blocks within the western Cordillera of Baja California to British Columbia. In *Geophysical Framework of the Continental United States,* eds L. C. Pakiser, W. D. Mooney. Geological Society of America Memoir. 172, pp. 471–492.

Beck, M. E., Jr, Burmester, R. F. and Schoonover, R. (1981) Paleomagnetism and tectonics of the Cretaceous Mt. Stuart Batholith of Washington: Translation of tilt? *Earth and Planetary Science Letters* **56,** 336–342.

Berg, H. C., Jones, D. L. and Richter, D. H. (1972) Gravina Nutzotin Belt-Tectonic significance of an upper Mesozoic sedimentary and volcanic sequence in southern and southeastern Alaska. *United States Geological Survey Professional Paper* **800-D,** D1–D24.

Berg, H. C., Elliott, R. L. and Koch, R. D. (1978) Geologic map of the Ketchikan and Prince Rupert quadrangles, southeastern Alaska. *United States Geological Survey Miscellaneous Investigations Map* **I-1807,** scale 1:250,000.

Berman, R. G. (1988) Internally consistent thermodynamic data for stoichiometric minerals in the system Na_2O–K_2O–CaO–MgO–FeO–Fe_2O_3–Al_2O_3–SiO_2–TiO_2–H_2O–CO_2. *Journal of Petrology* **29,** 445–522.

Berman, R. G. and Aranovich, L. Y. (1998) Optimized standard state and mixing properties of minerals: I. Model calibration for olivine, orthopyroxene, cordierite, garnet, and ilmenite in the system FeO–MgO–CaO–Al_2O_3–TiO_2–SiO_2. *Contributions to Mineralogy and Petrology* (in press).

Berman, R. G., Aranovich, L. Y. and Pattison, D. R. M. (1995) Reanalysis of the garnet–clinopyroxene Fe–Mg exchange thermometer. II. Thermodynamic analysis. *Contributions to Mineralogy and Petrology* **119,** 30–42.

Berman, R. G. (1991) Thermobarometry using multi-equilibrium calculations, a new technique with petrological applications. *The Canadian Mineralogist* **29,** 833–855.

Brew, D. A. and Ford, A. B. (1978) Megalineament in southeastern Alaska marks southwest edge of Coast Range batholithic complex. *Canadian Journal of Earth Science* **15,** 1763–1772.

Brew, D. A. and Ford, A. B. (1981) The Coast plutonic complex sill, southeastern Alaska. *United States Geological Survey Circular* **823-B,** B96–B99.

Butler, R. F., Gehrels, G. E., McClelland, W. C., May, S. R. and Klepacki, D. (1989) Discordant paleomagnetic poles from the Canadian Coast Plutonic Complex: Regional tilt rather than large-scale displacment. *Geology* **17,** 691–694.

Cohen, H. A. and Lundberg, N. (1993) Detrital record of the Gravina arc, southeastern Alaska: Petrology and provenance of Seymour Canal Formation sandstones. *Geological Society of America Bulletin* **105,** 1400–1414.

Cook, R. D., Crawford, M. L., Omar, G. I. and Crawford, W. A. (1991) Magmatism and deformation, southern Revillagigedo Island, southeastern Alaska. *Geological Society of America Bulletin* **103,** 829–841.

Cowan, D. S. (1994) Alternative hypotheses for the mid-Cretaceous paleogeography of the Western Cordillera. *GSA Today* **4,** 181, 184–186.

Cowan, D. S., Brandon, M. T. and Garver, J. I. (1997) Geologic tests of hypotheses for large coastwise displacements—a critique illustrated by the Baja British Columbia controversy. *American Journal of Science* **297,** 117–173.

Crawford, M. L. and Crawford, W. A. (1991) Magma emplacement in a convergent tectonic orogen, southern Revillagigedo Island, southeastern Alaska. *Canadian Journal of Earth Science* **28,** 929–938.

Crawford, M. L. and Hollister, L. S. (1982) Contrast of metamorphic and structural histories across the Work Channel lineament, Coast Plutonic Complex, British Columbia. *Journal of Geophysical Research* **87,** 3849–3860.

Crawford, M. L., Crawford, W. A. and Cook, R. D. (1989) Magmatism and tectonism, central Coastal Orogen, Alaska and British Columbia. *EOS Transactions of the American Geophysical Union* **70,** 1299.

Crawford, M. L., Hollister, L. S. and Woodsworth, G. J. (1987) Crustal deformation and regional metamorphism across a terrane boundary, Coast Plutonic Complex, British Columbia. *Tectonics* **6,** 343–361.

Crawford, M. L., Kraus, D. W. and Hollister, L. S. (1979) Petrologic and fluid inclusion study of calc-silicate rocks, Prince Rupert British Columbia. *American Journal of Science* **279,** 1135–1159.

Das, T., Rohr, K., Andronicos, C., Klepeis, K. and Hollister, L. (1996) 3-D Seismic reflection. Interpretation along the fiords crossing the boundaries of the Alexander accreted terrane, northern British Columbia. *Geological Society of America Abstracts with Programs* **28,** 650.

Davidson, C., Hollister, L. S. and Schmid, S. M. (1992) Role of melt in the formation of a deep-crustal compressive shear zone—the MacLaren Glacier metamorphic belt, south central Alaska. *Tectonics* **11,** 348–359.

Engebretson, D. C., Cox, A. and Gordon, R. G. (1985) Relative motions between oceanic and continental plates in the Pacific Basin. *Geological Society of America Special Paper* **206**.

Fuhrman, M. L. and Lindsley, D. H. (1988) Ternary-feldspar modeling and thermometry. *American Mineralogist* **73,** 201–216.

Gehrels, G. E., McClelland, W. C., Samson, S. D. and Patchett, P. J. (1991) U–Pb geochronology of the detrital zircons from a continental margin assemblage in the northern Coast Mountains, southeastern Alaska. *Canadian Journal of Earth Science* **28,** 1285–1300.

Gehrels, G. E. and Berg, H. C. (1988) A review of the regional geology and tectonics of southeastern Alaska. *United States Geological Survey Open-file Report* 88-659. scale 1:600,000.

Gehrels, G. E. and Berg, H. C. (1984) Geologic map of southeastern Alaska. *United States Geological Survey Open-file Report*. 84-886.

Gehrels, G. E. and Saleeby, J. B. (1987) Geologic framework, tectonic evolution, and displacement history of the Alexander terrane. *Tectonics* **6,** 151–173.

Gehrels, G. E., McClelland, W. C., Samson, S. D., Patchett, P. J. and Jackson, J. L. (1990) Ancient continental margin assemblage in the northern Coast Mountains, southeast Alaska and northwest Canada. *Geology* **18,** 208–211.

Holdaway, M. J., Mukhopadhyay, B. and Dutrow, B. L. (1995) Thermodynamic properties of stoichiometric staurolite $H_2Fe_4Al_{18}Si_8O_{48}$ and $H_6Fe_2Al_{18}Si_8O_{48}$. *American Mineralogist* **80,** 520–533.

Hollister, L. S. (1982) Metamorphic evidence for rapid (2 mm/yr) uplift of a portion of the Central Gneiss Complex, Coast Mountains, British Columbia. *The Canadian Mineralogist* **20,** 319–332.

Hollister, L. S. (1993) The role of melt in the uplift and exhumation of orogenic belts. *Chemical Geology* **108,** 31–48.

Hollister, L. S. and Crawford, M. L. (1986) Melt-enhanced deformation: a major tectonic process. *Geology* **14,** 558–561.

Hollister, L. S. (1977) The reaction forming cordierite from garnet, the Khatada Lake metamorphic complex, British Columbia. *Canadian Mineralogist* **15,** 217–229.

Hollister, L. S. and Andronicos, C. L. (1997) A Candidate for the Baja British Columbia Fault System in the Coast Plutonic Complex. *GSA Today* **7,** 1–7.

Hollister, L. S., Diebold, J., Lowe, C., Rohr, K., Humphreys, C., Smithson, S. B., Crawford, M. L., Crawford, W. A., Clowes, R. M., Ellis, R. M., Trehu, A. and Gehrels, G. E. (1994) Seismic image of the deep crustal structure of the Coast orogen of southeast Alaska and British Columbia. *Geological Society of America Abstracts with Programs* **26,** 146.

Hollister, L. S. and Crawford, M. L. (1990) Crustal formation at depth during continental collision. In *Exposed Cross-Sections of the Continental Crust*, eds M. H. Salisbury and D. M. Fountain, pp. 215–226. Kluwer Norwell, Massachusetts.

Hutchison, W. W. (1982) Geology of the Prince Rupert-Skeena map area, British Columbia. *Memoir of the Geological Survey of Canada* **394,** 1–116.

Ingram, G. M. and Hutton, D. H. W. (1994) The Great Tonalite Sill; emplacement into a contractional shear zone and implications for Late Cretaceous to early Eocene tectonics in Southeastern Alaska and British Columbia. *Geological Society of America Bulletin* **106,** 715–728.

Irving, E., Wheadon, P. M. and Thorkelson, D. J. (1993) Paleomagnetic results from the mid-Cretaceous Spences Bridge group and northward displacement of the eastern Intermontane Belt, British Columbia. *Geological Association of Canada Program and Abstracts*, A47.

Irving, E., Woodsworth, G. J., Wynne, P. J. and Morrison, A. (1985) Paleomagnetic evidence for displacement from the south of the Coast Plutonic Complex, British Columbia. *Canadian Journal of Earth Science* **22,** 584–598.

Jiang, D. and White, J. C. (1995) Kinematics of rock flow and the interpretation of geological structures with particular reference to shear zones. *Journal of Structural Geology* **17,** 1249–1265.

Lonsdale, P. (1988) Paleogene history of the Kula plate: offshore evidence and onshore implications. *Geological Society of America Bulletin* **100,** 733–754.

Ludwig, K. R. (1991a) ISOPLOT; a plotting and regression program for radiogenic-isotope data; version 2.53. *United States Geological Survey Open-file Report*, 91-445.

Ludwig, M. (1991b) ELLIROT; a program to view and analyze spatial distributions of ellipses. *Computers and Geosciences* **17,** 291–30.

McClelland, W. C., Gehrels, G. E., Samson, S. D. and Patchett, P. J. (1992) Structural and geochronologic relations along the western flank of the Coast Mountains batholith: Stikine River to Cape Fanshaw, central SE Alaska. *Journal of Structural Geology* **14,** 475–489.

McClelland, W. C. and Gehrels, G. E. (1990) Geology of the Duncan Canal shear zone: evidence for Early–Middle Jurassic deformation of the Alexander terrane, southeastern Alaska. *Geological Society of America Bulletin* **102,** 1378–1392.

Monger, J. W. H., Price, R. A. and Templeman-Kluit, D. J. (1982) Tectonic accretion and the origin of the two major metamorphic and plutonic welts in the Canadian Cordillera. *Geology* **10,** 70–75.

Price, N. J. and Cosgrove, J. W. (1990) *Analysis of Geological Structures*. Cambridge University Press, Cambridge.

Rubin, C. M. and Saleeby, J. B. (1992) Tectonic history of the eastern edge of the Alexander terrane, southeast Alaska. *Tectonics* **11,** 586–602.

Rubin, C. M., Saleeby, J. B., Cowan, D. S., Brandon, M. T. and McGroder, M. F. (1990) Regionally extensive mid-Cretaceous west-vergent thrust system in the northwestern Cordillera: implications for continental margin tectonism. *Geology* **18,** 276–280.

Rusmore, M. E. and Woodsworth, G. J. (1988) Eastern margin of the Coast plutonic complex, Mount Waddington map area, B.C.. *Geological Survey of Canada Paper* **88-1E,** 185–190.

Saleeby, J. B. and Rubin, C. M. (1989) The western margin of the Coast plutonic complex (CPC) in southernmost SE Alaska. *Geological Society of America Abstracts with Programs* **21,** 139.

Selverstone, J. and Hollister, L. S. (1980) Cordierite-bearing granulites from the Coast ranges, British Columbia: *P–T* conditions of metamorphism. *Canadian Mineralogist* **18,** 119–129.

Sisson, V. B. and Pavlis, T. L. (1993) Geologic consequences of plate reorganization: an example from the Eocene southern Alaska forearc. *Geology* **21,** 913–916.

Stacey, J. S. and Kramers, J. D. (1975) Approximation of terrestrial lead isotope evolution by a two-stage model. *Earth and Planetary Science Letters* **26,** 207–221.

Stock, J. and Molnar, P. (1988) Uncertainties and implications of the Late Cretaceous and Tertiary position of North America relative to the Farallon, Kula and Pacific plates. *Tectonics* **7,** 1339–1384.

Tobisch, O. T., Saleeby, J. B., Renne, P. R., McNulty, B. and Weixing, T. (1995) Variations in deformation fields during development of a large-volume magmatic arc, central Sierra Nevada, California. *Geological Society of America Bulletin* **107,** 148–166.

Umhoefer, P. J., Dragovich, J., Cary, J. and Engebretson, D. C. (1989) Refinements of the "Baja British Columbia" plate-tectonic model for northward translation along the margin of western North America. In *Structure and Past Kinematics of Accreted Terranes*, ed. J. W. Hillhouse, American Geophysical Union. Geophysical Monograph **50,** 101–111.

Umhoefer, P. J. (1987) Northward translation of "Baja-British Columbia" along the Late Cretaceous to Paleocene margin of western North America. *Tectonics* **6,** 377–394.

Wood, D. J., Stowell, H. H., Onstott, T. C. and Hollister, L. S. (1991) $^{40}Ar/^{39}Ar$ constraints on the emplacement, uplift, and cooling of the Coast Plutonic Complex sill, southeastern Alaska. *Geological Society of America Bulletin* **103,** 849–860.

APPENDIX

U–Pb isotope methodology

All U–Pb samples were processed using a jaw crusher, roller crusher, Wilfley table, heavy liquids, and Frantz magnetic separator. Analytical techniques are described in more detail by Gehrels *et al.* (1991). The non-magnetic zircons were sieved into size fractions and then selected for analysis based on optical properties using a binocular microscope. We selected grains with few fractures, inclusions, and cores, and highly elongate rods where possible. Selected zircons then were dissolved in $HF > HNO_3$ in 0.01 ml Teflon microcapsules within a 125 ml dissolution chamber during a period of 30 h at 245°C. The solutions were evaporated to dryness, a $^{205}Pb/^{235-233}U$ spike was added, and the precipitate was dissolved in the dissolution chamber in 3.1 N HCl for 8 h at 225°C.

Isotope analyses were conducted with a VG-354 mass spectrometer equipped with six Faraday collectors and an axial Daly detector. The measurements were made in computer-controlled dynamic mode, with the Daly detector used simultaneously with the Faraday collectors to measure ^{204}Pb. The gain factor of the Daly detector was determined continuously by comparing $^{206}Pb_{(Faraday)}/^{207}Pb_{(Faraday)}$ with $^{206}Pb_{(Faraday)}/^{207}Pb_{(Daly)}$. Finally, isotopic data were processed utilizing data reduction and plotting programs of Ludwig (1991a, b).